Applied Catalysis B: Environmental 343 (2024) 123455

Contents lists available at ScienceDirect

Applied Catalysis B: Environmental

journal homepage: www.elsevier.com/locate/apcatb

Selective glucose oxidation to glucaric acid using bimetallic catalysts: Lattice expansion or electronic structure effect?

Žan Lavrič [a,f,1], Janvit Teržan [a,b,*,1], Ana Kroflič [a], Janez Zavašnik [c], Joanna Elżbieta Olszówka [d], Štefan Vajda [d], Matej Huš [a,e,f], Miha Grilc [a,f], Blaž Likozar [a,g]

[a] Department of Catalysis and Chemical Reaction Engineering, National Institute of Chemistry, Hajdrihova 19, SI-1000 Ljubljana, Slovenia
[b] Department of Synthesis of Materials, Jožef Stefan Institute, Jamova Cesta 39, 1000 Ljubljana, Slovenia
[c] Gaseous Electronics, Jožef Stefan Institute, Jamova Cesta 39, 1000 Ljubljana, Slovenia
[d] Department of Nanocatalysis, J. Heyrovský Institute of Physical Chemistry v.v.i., Czech Academy of Sciences, Dolejškova 2155/3, CZ-182 23 Prague 8, Czech Republic
[e] Institute for the Protection of Cultural Heritage of Slovenia (ZVKDS), Poljanska cesta 40, SI-1000 Ljubljana, Slovenia
[f] University of Nova Gorica, Vipavska 13, SI-5000 Nova Gorica, Slovenia
[g] Faculty of Polymer Technology, Ozare 19, SI-2380 Slovenj Gradec, Slovenia

ARTICLE INFO

Keywords:
Glucaric acid
Glucose oxidation
Catalyst characterization
DFT
Microkinetic modelling

ABSTRACT

Our study presents a comprehensive approach for the selective oxidation of glucose to glucaric acid (GA) by heterogeneous catalysis. We have synthesized and characterized Au/ZrO_2, AuCu/ZrO_2 and AuPt/ZrO_2 catalysts using X-ray diffraction (XRD), transmission electron microscopy (TEM), X-ray photoelectron spectroscopy (XPS), and oxygen pulse chemisorption (OPS) techniques. Combining experimental observations with in-depth density functional theory (DFT) studies, we found that bimetallic catalysts form alloys, which exhibit different characteristics than monometallic counterparts for the given reaction. We performed batch reactions, varying temperature and oxygen pressure, and used the data to construct a predictive microkinetic model. As it turned out, AuPt/ZrO_2 showed the highest selectivity, yielding 32% of GA at 100 °C and 30 bar_g O_2. Our results provide valuable insights for the developing of efficient catalysts and point out the bottlenecks for the oxidation of glucose to GA.

1. Introduction

The growth of our society, the limited supply of fossil fuels, and the environmental impact of current industrial technologies have driven research into bio-based and renewable chemical feedstock. In this sense, biomass conversion has gained increasing attention in the last two decades[1–3], because of the incredible variety of materials which can be obtained [4].

Waste from lignocellulosic biomass is the most abundant renewable source of organic carbon [5]. Its decomposition into individual monomers such as glucose is well understood, but its further conversion into value-added chemicals remains challenging. Glucose is an essential feedstock that can be converted into several beneficial compounds by hydrogenation, dehydration or fermentation. One of the promising biomass-derived compounds, recognized by the U.S. Department of Energy, is glucaric acid (GA)[6,7]. The latter is a very important renewable ingredient in liquid detergents, a substitute for phosphates (demand for GA has increased dramatically since the ban on the use of phosphates), and is also used in the food, pharmaceutical, and chemical industries (important intermediate in the production of bio-based adipic acid).[8–13] Despite its importance, no scalable and cost-effective technology has yet been developed to meet the growing market demand.

GA is industrially obtained by glucose oxidation with nitric acid and/or bleaching agents, which is technologically demanding and not ecological [14,15]. Although alternative methods such as electrocatalytic and photocatalytic oxidation, [16–18] fermentation and enzymatic biotransformation,[19–23] or oxidation using TEMPO or related nitroxyl radical oxidants [24–29] have been proposed, glucose oxidation with nitric acid remains the most economical method, due to the low price of the oxidant. Another promising method for obtaining

* Corresponding author at: Department of Catalysis and Chemical Reaction Engineering, National Institute of Chemistry, Hajdrihova 19, SI-1000 Ljubljana, Slovenia.
E-mail address: janvit.terzan@ki.si (J. Teržan).
[1] The authors contributed equally to the manuscript.

https://doi.org/10.1016/j.apcatb.2023.123455
Received 22 September 2023; Received in revised form 27 October 2023; Accepted 30 October 2023
Available online 8 November 2023

GA is the direct oxidation of glucose with air/oxygen and metal catalysts on supports. The oxidation of glucose to gluconic acid (GU) (only the aldehyde group is oxidised) in an aqueous solution is a well-studied reaction[30–32], which is most successfully carried out with Au-based catalysts [33–39]. The studies of the conversion of lignocellulosic biomass to value-added chemicals have been expanded to bimetallic catalysts as well [40]. On the other hand, the pathway of oxidation of glucose in aqueous solution to GA using molecular oxygen has not been fully elucidated. Originally, the reaction was carried out under alkaline conditions using platinum-based mono- and bimetallic catalysts, and a maximum yield of 54% was achieved with a Pt/C catalyst.[41] However, at higher conversion rates, an undesirable additional reaction occurs, releasing free acids from their salts. Therefore, studies on the base-free process gained much more interest.[42–44]. The reactions were carried out in laboratory-scale reactors under high O_2 partial pressure (27-bar_g), with GA yields up to 70%.[42] The activity of the Pt-, Pt-Au supported metals was confirmed when the laboratory scale reaction was carried out at neutral pH, resulting in even higher yields of up to 74% [43,45–47]. The study on the effect of support, reaction pH, O_2 pressure, and metal loading showed the importance of all of these parameters[43,46,48]. Moreover, the synergistic effect of each metal in bimetallic catalysts was discussed in several studies, indicating the superiority of bimetallic over monometallic catalysts due to the formation of the favourable electronic effect [37,38,46,49,50]. The latter is signified by a difference in the surface electron density, which can facilitate oxygen activation and furthermore oxidation of the terminal alcohol. Several studies focusing on the comparison between mono- and bimetallic catalysts were published [51], where the bimetallic materials outperformed their monometallic counterparts. However, a clear reason for this phenomenon has never before been clearly described. The benefit of bimetallic particles in glucose conversion was recently reported by Gao et al.[52], who demonstrated a clear benefit in using PtNi alloy for the hydrogenation of glucose.

The literature on the mechanism and kinetic aspects of glucose oxidation mainly focuses on the reaction step to GU, [53–58] while further studies on oxidation to GA are relatively scarce. Moreover, challenges such as the low selectivity for GA or the harsh reaction conditions (high O_2 partial pressure or long reaction time) [49] still need to be addressed to achieve a technological breakthrough.

In this work, a catalytic study of heterogeneous glucose oxidation on gold-based mono- and bimetallic ZrO_2-supported catalysts (Au, AuCu, and AuPt) is presented. The synthesised catalysts were analysed by transmission electron microscopy (TEM), oxygen pulse chemisorption (OPS), X-ray diffraction (XRD) and X-ray photon spectroscopy (XPS) to determine the surface properties of the synthesised catalysts. Later, batch experiments were performed at different reaction times, temperatures, and partial oxygen pressures. Based on the obtained results, we developed a microkinetic model to study the complex reaction pathway in detail and to unravel the rate-limiting steps of the process itself for the whole reaction pathway, from glucose to GA. The observed differences in catalytic performance were additionally explained with DFT calculations, which revealed the importance of varying oxophilicity of different catalysts and accessible active oxygen species.

2. Materials and methods

2.1. Catalyst Synthesis

Synthesis of catalysts: In a typical synthesis, 2 g of the support (ZrO_2) was dispersed in 40 mL of deionized H_2O (dH_2O) (18.2 MΩ). In addition, 279.9 mg of $HAuCl_4$ x 3 H_2O was dissolved in 10 mL of dH_2O to load the catalyst with 7 wt% gold. This solution was added dropwise to the dispersed support under vigorous stirring. After 10 min, the pH was raised to 8 by adding 2.5% NH_4OH solution. The suspension was stirred for another 2 h at room temperature. Then 160 μL of hydrazine hydrate (80% aqueous solution) was added to reduce the metal ions. The loaded catalyst was collected by centrifugation, and the supernatant was discarded and re-dispersed in dH_2O. This procedure was repeated 3 more times to wash the catalyst thoroughly. For the bimetallic catalysts, the procedure was identical, except that 50 mol% of Au was replaced with the appropriate metal. The weights were 119.7 mg $PtCl_4$, 85.9 mg Cu $(NO_3)_2$ x 3 H_2O, and the catalysts were denoted as Au, AuPt and AuCu.

2.2. Catalyst characterisation

The phase composition of the crystalline samples was determined by X-ray powder diffraction (PANalytical X'Pert PRO) at 45 kV with a CuKα1 radiation source between 10° and 90°, a step size of 0.05, and a counting time of 500 s. The recorded diffractograms were interpreted with the Profex software package (ver. 5.1.0) using crystal structure data from the Crystallography Open Database (COD).

The crystal structure and morphology of the nanoparticles were analysed by transmission electron microscope (TEM, JEM-2100, JEOL Inc.) operating at 200 kV. The micrographs were recorded by a slow-scan CCD camera (Orius SC1000, Gatan Inc.) and analysed with DigitalMicrograph software (ver. 3.01.598.0, Gatan Inc.). The powder catalysts were dispersed in EtOH(abs) and sonicated for 30 s in an ultrasonic bath to prevent aggregation. The solution was dropped onto commercially available amorphous carbon Ni-supported grids and mounted in a double-tilt low-background Be holder.

Pulse chemisorption and TPD experiments were performed with the four catalysts using the Micrometrics AutoChem II Chemisorption Analyser (Micrometrics, Norcross, GA, USA). The catalysts were pretreated for 2 h in an Ar atmosphere at 120 °C. After pretreatment, the materials were exposed to 15 pulses of 10% O_2 in He (Messer, Bad Soden am Taunus, Germany).

We performed X-ray photoelectron spectroscopy (XPS) to determine whether the alloy leads to a shift in the binding energy of Au 4 f. The latter would indicate an altered ability of the nanoparticles to activate the reactants. The resolution of the analyser is 0.65 eV. The analysis was performed with the PHI VersaProbe 3 AD (Phi, Chanhassen, US), which uses a monochromatic Al Kα X-ray source. For charge neutralisation, the charge of the sample was attenuated with two beams (electrons and ions). The peak shift caused by the neutralisation was corrected by shifting the peaks of the adventitious carbon species to 284.8 eV. We measured the survey spectra at a transit energy of 224 eV with a step of 0.8 eV. The high-resolution spectra were measured with a transite energy of 27 eV and a step size of 0.05 eV. For the survey spectra, 2 sweeps were performed, while for the high-resolution spectra, 20 sweeps were performed. The spectral deconvolution was performed with the Multipak software.

2.3. Glucose oxidation experiments

Catalytic activity tests were performed using six parallel 75 mL stainless steel batch reactors (Parr 5000 series) mixed with a magnetic stirrer set at 600 rpm. Each batch system was equipped with a liquid phase sampling line to allow sampling of the liquid phase during the reaction period. The reaction mixture comprised 40 mL of 0.25 M aqueous glucose and 750 mg of catalyst. The concentration and mass were chosen so that the glucose to active metal ratio was equal to 40. Before the reaction, each autoclave was purged three times with N_2 (5.0, Messer, Bad Soden am Taunus, Germany), once with oxygen (Messer, Bad Soden am Taunus, Germany) and then pressurised with oxygen to 16 or 30 bar gauge (5.0, Messer, Bad Soden am Taunus, Germany).

2.4. Liquid phase analysis

HPLC was used to determine the extent of glucose oxidation. It was performed using a Thermo-Fisher Scientific UltiMateTM 3000 UHPLC with DAD and RI. The column used was the Rezex RHM-Monosaccharide H+ with a guard column of the same type. The mobile phase was pure

water (18.2 MΩ). The column was maintained at 60 °C with a flow of 0.6 mL min^{-1}. Detection was performed using the RI detector.

Ionic chromatography (IC) was used to determine gluconic, glucuronic, glucaric, tartaric, tartronic, glycolic, oxalic, and formic acid. Acidic reaction products were determined using a Dionex ICS 3000 ion chromatograph equipped with an eluent generator, a suppressor, and a conductivity detector. Samples were collected at predefined times during the reaction and refrigerated until dilution with MilliQ water, filtration, and analysis. Satisfactory separation of analytes was achieved on a Dionex IonPac AS11-HC, 4 × 250 mm analytical column in combination with an appropriate precolumn (Dionex IonPac AG11-HC, 4 ×50 mm). A KOH gradient was used, starting at 2 mM for 8 min, followed by a 25 min stepwise increase to 35 mM KOH and then rinsing with 100 mM KOH before injection of the next sample. The injection volume was 10 μL, the flow rate was 1 mL min^{-1}, and the column temperature was 35 °C.

2.5. Microkinetic model

In order to develop a microkinetic model, a detailed reaction pathway had to be constructed with all reactants, stable intermediates and products detected during the catalytic activity tests. In this manuscript, we propose a tentative reaction network (vide infra), which includes only stable intermediates. Since the microkinetic modelling was performed based on experimental data, elementary reactions *cannot* be included. The colour of each compound (except carbon dioxide) corresponds to the line colour in the graphs of concentration and time below.

The purpose of the model is to describe a three-phase reaction system, where oxygen solubility is in thermodynamic equilibrium at the gas-liquid interface, competitive adsorption and desorption of all compounds and the catalytic reaction on the catalyst active surface sites. We calculated the concentration of reactants, intermediates, and products by solving a set of ordinary differential equations (ODE), based on the proposed reaction pathway regarding the following assumptions:

1. Under the reaction conditions applied, without metallic particles present in the catalyst formula, there was no conversion. Therefore, it is assumed that the reactions only occur on the surface of the metallic nanoparticles.
2. Vacant sites suitable for adsorption are all equivalent and independent of the overall coverage.
3. Each active (metal) site is covered by one organic or oxygen molecule at a time since they adsorb competitively.
4. Adsorption and desorption constants of all organic molecules are equivalent as they have a similar structure. The mentioned constants are also a few orders higher than the surface reaction, to simulate the reaction mechanism without internal or external mass transfer resistance, which is not present, since the ZrO_2 powder used as supporting material is submicron in size and relatively non-porous. This means that the experiments were performed in such a manner, where surface reaction rates govern the overall kinetic regime.
5. The solubility of oxygen is calculated using Henry's law at operating reaction conditions (60–120 °C, 16 – 30-bar gauge O_2).

The adsorption rate (r_j^{ads}) of each compound *j* depends on the adsorption rate constant (k_j^{ads}), its concentration in a liquid phase (C_j^L) and the concentration of vacant sites (Θ_{vs}), defined in Eq. (1).

$$r_j^{ads} = k_j^{ads} \bullet C_j^L \bullet \Theta_{vs} \tag{1}$$

The desorption rate (r_j^{des}) of each compound *j* depends on the desorption rate constant (k_j^{des}), coverage of *j*, adsorbed on the active sites (Θ_j) and moles of all active sites (n_{TS}), defined in Eq. (2).

$$r_j^{des} = k_j^{des} \bullet \Theta_j \bullet n_{TS} \tag{2}$$

The surface reaction rate (r_j^{surf}) of all compounds depends on the surface reaction rate constant (k_j^{surf}), the compound coverage on the catalyst surface (Θ_j), the concentration of oxygen (if oxygen is required for the reaction to take place) on the surface (Θ_{O2}) and moles of all active sites (n_{TS}), defined in Eq. (3).

$$r_j^{surf} = k_j^{surf} \bullet \Theta_j \bullet \Theta_{O_2} \bullet n_{TS} \tag{3}$$

Temperature and pressure data were recorded during the experiment to calculate mass transfer rates, reaction rate constants and thermodynamic properties such as oxygen solubility. In contrast, adsorption and desorption constants were assumed to be temperature independent and much higher than much slower reaction rate constants. The impact of temperature on the surface reaction rate constants was applied to follow the Arrhenius law, as shown in Eq. (4).

$$k_j^{surf}(T_2) = k_j^{surf}(T_1) \bullet \exp\left(\frac{Ea_i}{R} \bullet \left(\frac{1}{T_1} - \frac{1}{T_2}\right)\right) \tag{4}$$

The differential balance equations with respect to the assumed reaction network are as follows (Eqs. 5–9):

The general oxygen balance in the gaseous phase is shown by Eq. (5).

$$\frac{dn_{O_2}^G}{dt} = -k_{GL}a \bullet \left(\frac{p_{O_2}}{He} - C_{O_2}^L\right) \tag{5}$$

The general balances of compounds in the liquid phase are calculated by Eq. (6), where V_L is the volume of the liquid phase.

$$\frac{dC_j^L}{dt} = -r_j^{ads} + \frac{r_j^{des}}{V_L} \tag{6}$$

The general oxygen balance in the liquid phase is calculated by Eq. (7).

$$\frac{dC_{O_2}^L}{dt} = k_{GL}a \bullet \left(\frac{p_{O_2}}{He} - C_{O_2}^L\right) \bullet \frac{1}{V_L} - r_j^{ads} + \frac{r_j^{des}}{V_L} \tag{7}$$

The general balance for the active site coverage is calculated by Eq. (8).

$$\frac{d\Theta_j}{dt} = \left(r_j^{ads} \bullet V_L - r_j^{des} + \Sigma_j^n \pm r_j^{surf}\right) \frac{1}{n_{TS}} \tag{8}$$

The general balance for vacant sites is calculated by Eq. (9).

$$\frac{d\Theta_{vs}}{dt} = \left(-V_L \bullet \Sigma_j^n r_j^{ads} + \Sigma_j^n r_j^{des} + \Sigma_j^n \pm r_j^{surf}\right) \frac{1}{n_{TS}} \tag{9}$$

The turnover frequency for each reaction is calculated by Eq. (10).

$$TOF = \frac{k_i(T) \bullet \theta_j(t) \bullet \theta_k(t)}{mass \quad of \quad active \quad metal} \tag{10}$$

We use MATLAB 2021b software to solve the formulated system numerically. The concentration profiles were solved as a function of time with ODE23tb solver, an implicit Runge-Kutta formula, with a trapezoidal rule step as its first stage and a backward differentiation formula of order two as its second stage. Initial concentrations of all compounds were set to zero, except for glucose concentration in the liquid phase and the oxygen partial pressure in the gas phase.

2.6. Quantum chemical calculations

First-principle simulations were carried out with the Vienna Ab Initio Simulation (VASP) programme v5.4.1 with the VTST tools [59–61]. To describe the exchange correlation, the revised PBE functional (RPBE) [62] was used. A GGA approach was adequate since catalytic surfaces were metallic. To account for the dispersion interaction, poorly reproduced by GGA, a Grimme D3 correction was employed [63].

Electron-core interaction was described with the projector-augmented wave pseudopotential [64,65]. It was found an energy cut-off of 450 eV sufficed for well converged results. A force threshold of

0.03 eV/Å was used in converging energy-minimum structures and saddle points, which were located using the dimer method [66,67]. They were confirmed with a vibrational analysis using the finite difference approach with a step of 0.01 Å.

All simulated metals were described as extended surfaces (111 for fcc metals) with four-layer slabs, the bottom two being frozen to their bulk positions (see SI for lattice parameters obtained by energy optimizations of their unit cells). The slabs were sampled at a gamma point because of their size, totalling 100 atoms (5 × 5 supercells). The conventional approach to estimating adsorption, reaction and activation energies was used:

$$E_{ads} = E_{adsorbed} - E_{adsorbate} - E_{catalyst} \quad (10)$$

$$\Delta E = E_{products} - E_{reactants} \quad (11)$$

$$E_A = E_{TS} - E_{reactants} \quad (12)$$

3. Results

3.1. Powder X-ray diffraction (XRD)

The crystal structure and phase composition of the synthesised materials were first analysed by XRD. Most diffraction peaks belong to the baddeleyite - monoclinic ZrO_2, S.G. $P12_1/c1$ [68]. After loading the materials with Au, an additional peak appeared at 38.1°2θ, corresponding to standard Bragg reflections of *fcc* Au (111). The samples loaded with mixed AuPt or AuCu show no characteristic peaks for the pure Pt or Cu phase that would indicate a separate deposition of each metal, suggesting a formation of mixed Au-Pt and Au-Cu compounds (Fig. 1). For the AuPt mixture, a small peak at 39°2θ coincides with theoretical diffraction for the AuPt compound with a 1:1 ratio. For the AuCu mixture, an expected diffraction peak at 40.7°2θ coincides with the $ZrO_2(-211)$ peak and cannot be further resolved.

3.2. Transmission electron microscopy (TEM)

The powdered samples were analysed by transmission electron microscope (TEM). The irregularly shaped ZrO_2 template particulates are stable under the electron beam and are up to 1 μm in size. As already identified by XRD, their crystal structure corresponds to baddeyelite, the most stable monoclinic ZrO_2 polymorph. Upon closer look, we can see that the ZrO_2 template is covered by nano-sized metal particles, easily resolved even by contrast (are darker than ZrO_2, Fig. 2). For pure Au-loaded sample, the Au NPs are spherical and rounded, without clearly formed Wulff facets, having a typical multiple-twinned crystal structure (Fig. 2a). The measured cell parameters calculated from selected area electron diffraction (SAED) patterns correspond with theoretical values for pure *fcc* Au (cubic, Fm-3 m, a = 4.08 Å) [69]; this data was further used as an internal standard for the calibration of the SAED (TEM camera length) for the samples with bimetallic loading.

In the AuPt-loaded sample, the metallic particles appear uniformly scattered over the ZrO_2 template, with a narrow size distribution and are somewhat smaller compared to pure Au loading. The crystals have well-developed icosahedral morphology and appear to have a homogenous composition (Fig. 2b). The lattice parameters, measured from HR-TEM micrographs and diffraction patterns, are ~2.5% smaller as for pure *fcc* Au; a(4.00 Å) compared to a(4.08 Å), respectively (Fig. 2d). Based on Vegard's law, the measured experimental values of lattice constant correspond to bimetallic composition for alloyed AuPt nanoparticles with approx. 50:50 ratio. Such crystal structure corresponds to a typical alloy, a non-ordered mixture of *fcc*(Au) + *fcc*(Pt) component [70].

Similar observations were made in the case of AuCu loading. Here, the metal particles are scattered over the ZrO_2 template. The size distribution of the metal particles does not seem very homogeneous - the larger particles are comparable to those of the AuPt sample, while the majority are smaller. The individual particles have a well-defined Wulff shape and show numerous internal defects, such as Σ3-type twinning. Their crystal structure was analysed using HR-TEM and SAED. We measured the lattice spacing of the randomly selected single-crystal particles, which are between the monometallic Au (4.08 Å) and Cu (3.61 Å), corresponding to a disordered *fcc* AuCu binary alloy [71]. The Au-Cu phase diagram is complex, and consists of *fcc* AuCu solid solution and several intermetallic phases, such as tetragonal AuCu-I, and orthorhombic AuCu-II phases [72]. In the operational temperature window of

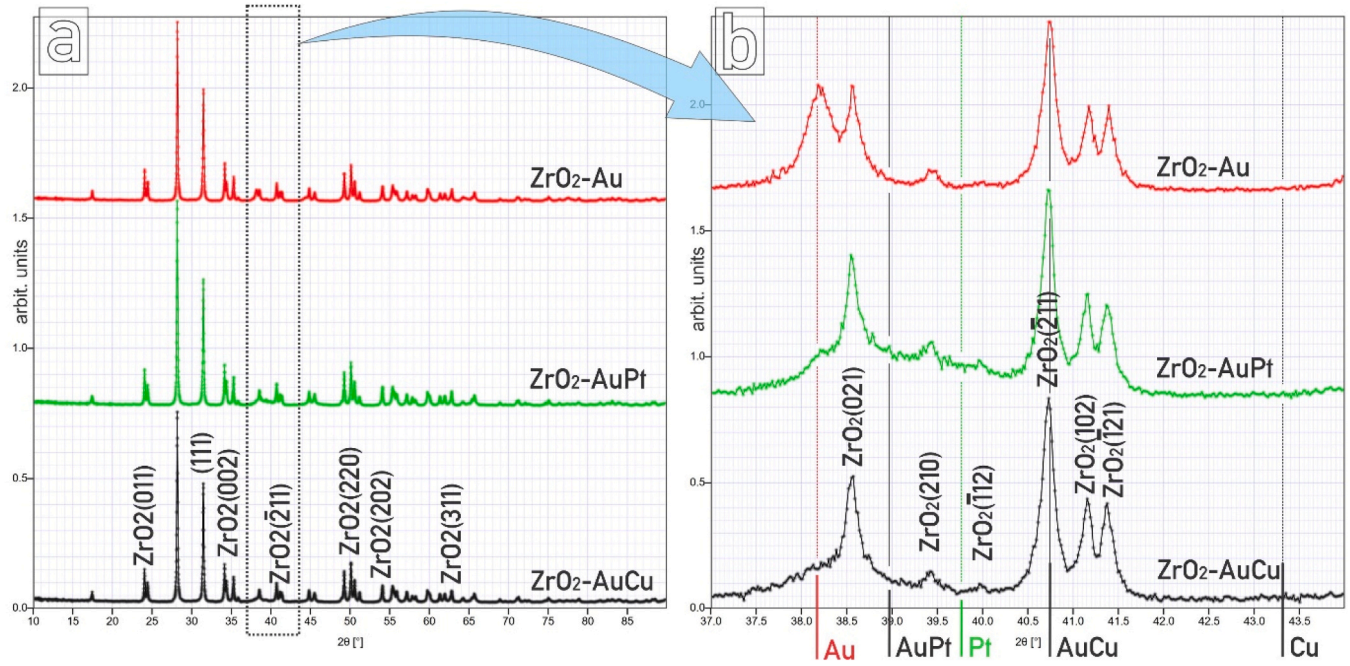

Fig. 1. (a)The overlaid XRD spectra of the three synthesised compound materials; the main diffraction peaks are indexed for baddeleyite (monoclinic ZrO_2). (b) Magnified marked region between 37° and 44°2θ, with the marked simulated peak positions for Au (111), Pt (111) and Cu (111), as well as the theoretical reflections for the AuPt and AuCu alloys.

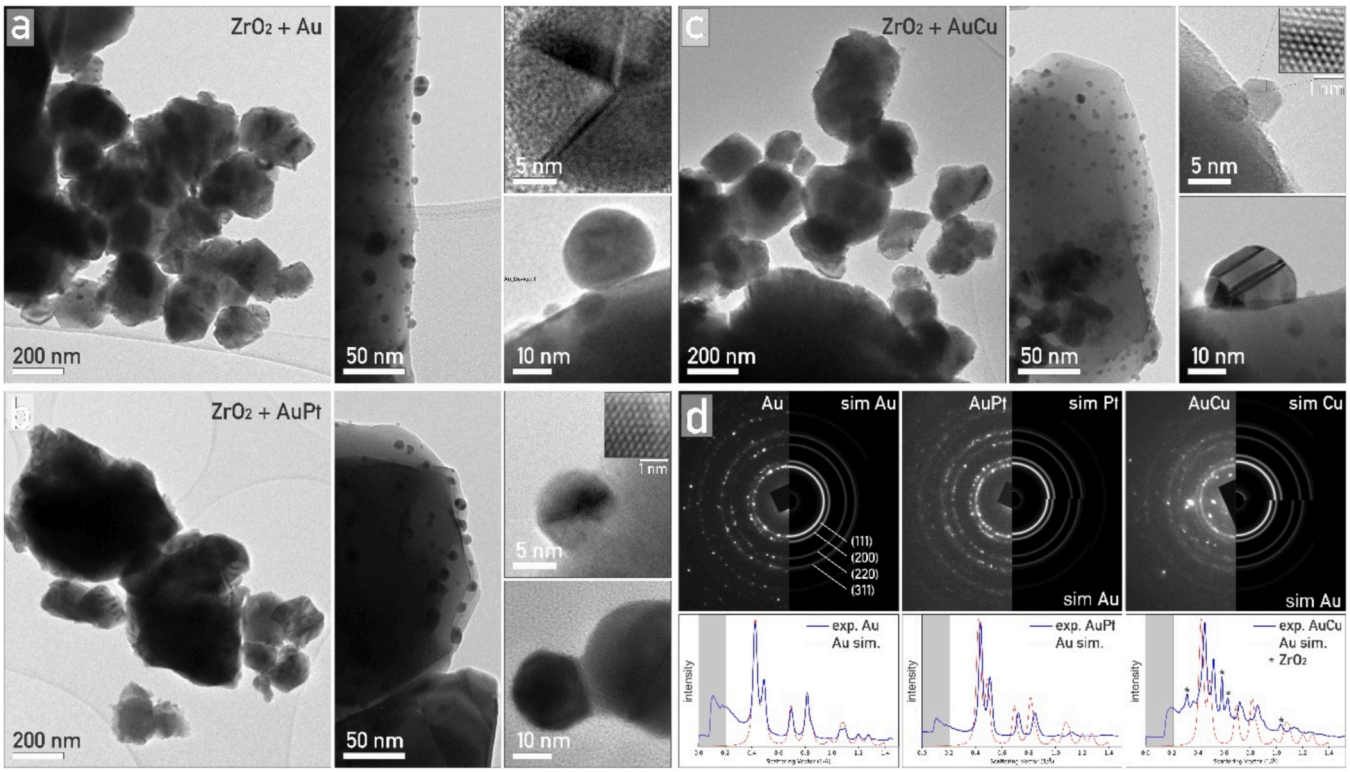

Fig. 2. TEM micrographs of ZrO_2 substrate with (a) Au, (b) AuPt, and (c) AuCu loading. The metal NPs can be easily identified by higher mass and diffraction contrast. (d) A comparison of experimental SAED patterns and ab initio simulations for pure Au, Pt and Cu, with corresponding intensity profiles.

our experiment, the structure of AuCu alloy in 50:50 ratio after homogenization is reported to be tetragonal (c/a ~ 0.92, P4/mmm, a=2.80 Å) and is stable up to 350 °C [73]. With the results of SAED for both bimetallic materials we confirmed the formation of the AuPt and AuCu alloys. We used the average particle diameter measured by TEM to determine the dispersion. The latter was calculated using the equation reported by Borodziński and Bonarowska [74] using atomic radii reported in the literature [75,76]. The calculated dispersions are very similar to numbers put forth by Bergeret and Gallezot [77]. These results were used to define the active sites available for glucose adsorption, which were used in the microkinetic model.

3.3. Oxygen pulse chemisorption

Oxygen binding capacity is a crucial parameter in glucose oxidation. To determine the latter, we performed oxygen pulse chemisorption. Chemisorption was performed at 120 °C, as this is the highest temperature at which we performed glucose oxidation. The amount consumed by each material was normalised per gram of active metal. The experiments clearly show that alloying gold with copper or platinum dramatically increases the amount of oxygen that binds to the surface of the catalysts (Fig. 3). This is particularly clear with the AuPt bimetallic material, where the increase is more than 2.5 times (89–230 μmol). These experimental results correlate very nicely with first-principle insights, which show a noticeably lower activation energy for dissociative oxygen adsorption on Cu and Pt (vide infra). A similar observation was also noted by Gottfried et al., who found that O_2 adsorbs very poorly on pure Au.

3.4. X-ray photoelectron spectroscopy (XPS)

From the survey spectra, we confirmed that all the nominal metals are indeed present in the final materials. The charge-corrected results of XPS show that pure Au is positioned at 84.0 eV [78]. The peaks were

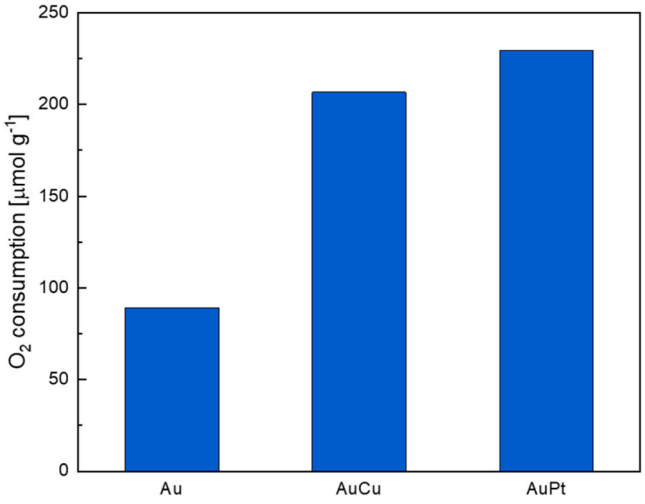

Fig. 3. The results of oxygen pulse chemisorption. The amounts are normalised per gram of active metal, or metals in the case of bimetallic catalysts.

fitted with the Multipak software, using asymmetric peak shapes and the smart baseline option. We observed the split spin-orbit components, with a split of 3.7 eV. When Au was alloyed with Pt, the shift was negligible, resulting in a shift below 0.1 eV. On the other hand, the shift is much more prominent when gold is alloyed with copper (Fig. 4). This could be the result of Cu oxidation, which is clearly visible due to the well-pronounced satellite at 943 eV. The electronegativity of Cu is significantly lower than that of Au. Therefore, we would expect a shift to lower binding energies in the Au 4 f peak for Au. However, with the surface oxidation of Cu, where the electronegativity of O is significantly higher than that of Au, a shift to higher binding energies is reasonable. Since the difference in shift is negligible when Au is alloyed with Pt, we

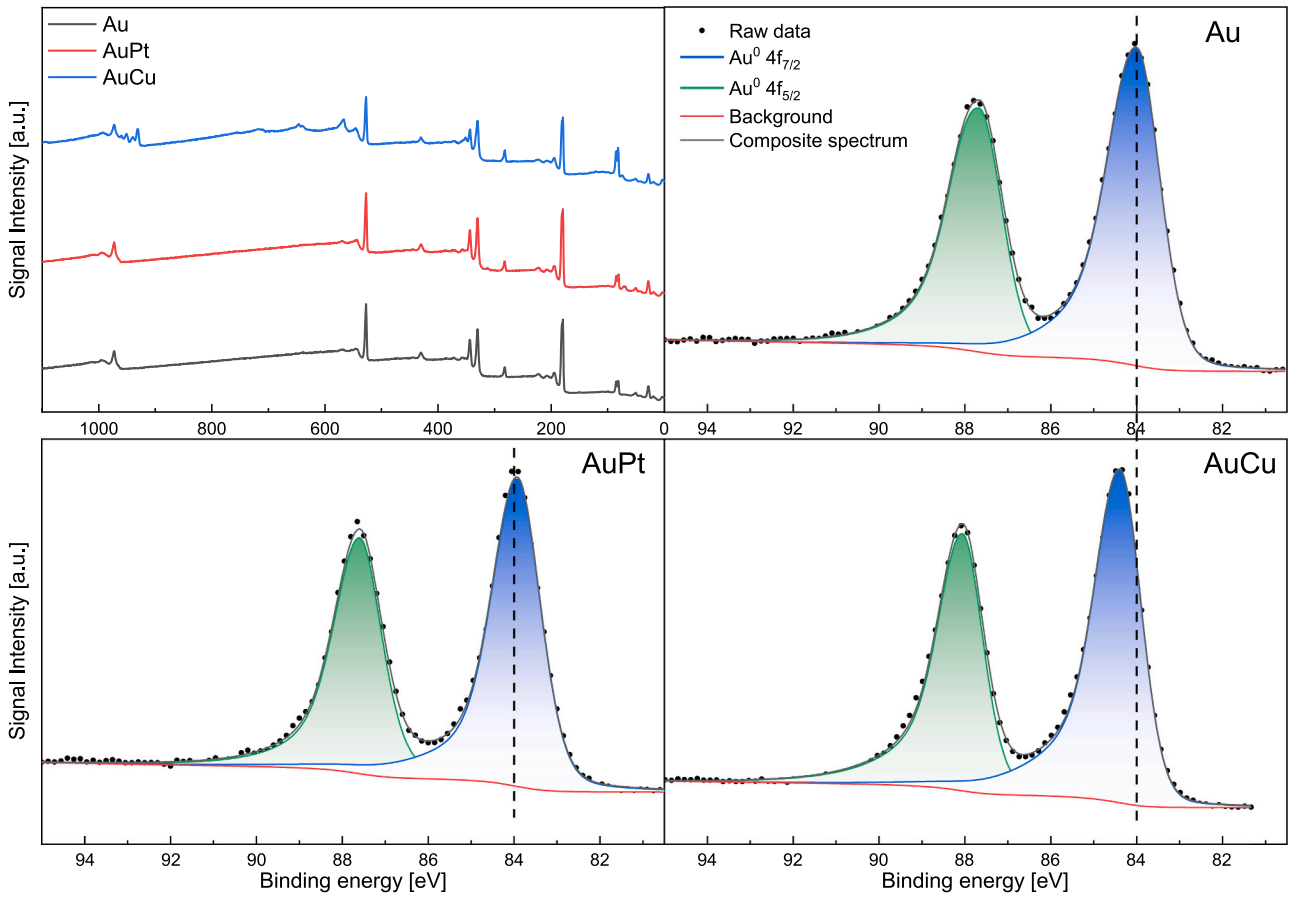

Fig. 4. The survey XPS spectra measured for the three materials synthesised for this study and the 4 f region of Au, which indicates the gold is only present in metallic form. The vertical dashed line is positioned at 84.0 eV, indicating the position of pure Au 4 $f_{7/2}$.

believe the any shift is due to the interaction of Au with the other metal. When Au is alloyed with Pt, a slight shift is expected because the difference in electronegativity of the two elements is small. The region at 71.0 eV associated with Pt 4 $f_{7/2}$ shows that Pt is in the metallic state and that the shift is negligible. This coincides well with the minimal shift in the binding energy of Au 4 f.

3.5. Catalytic investigation of selective glucose oxidation

Liquid products analysed by HPLC and IC for glucose oxidation with the above-mentioned catalysts, under the applied reaction conditions, revealed that the most important intermediates and products are: gluconic acid (GU), glucuronic acid (GLU), glucaric acid (GA), tartaric acid (TA), tartronic acid (TO), glycolic acid (GLY), oxalic acid (OX), and formic acid (FA). Two intermediates reported in previous studies [46], using a similar AuPt catalyst, 2-keto-D-gluconic acid and 5-keto-D-gluconic acid, were not detected.

Additionally, Weisz Prater and Mears parameters were calculated, to determine if there is any internal or external mass transfer limitations. Weisz Prater parameter for Glc oxidation was determined to be 1.4×10^{-8}, which means internal mass transfer limitation was not present. Moreover, Mears parameter for Glc oxidation was determined to be 1.39×10^{-11}, also confirming that external mass transfer resistance did not affect reaction kinetics. In other words, particle diameter of ZrO_2 supporting material was determined to be around 1 μm, which is relatively small. Determined from Brunauer-Emmett-Teller (BET) analysis [79], the porosity of the catalytic microparticles was determined to be 0.08, which indicates low porosity and corroborates the low Weisz Prater and Mears parameter. The calculation of each parameter is described in detail in supplementary information (SI). Moreover, the observed hysteresis loops, obtained from nitrogen sorption experiments, for supporting material ZrO2 and all the synthesized catalysts are shown in Fig. S3. The isotherms presented in Fig. S3 can be classified as a type IV(a) isotherm with type H3 hysteresis loop, proving that the material is nonporous. Finally, the surface area of the materials is affected negligibly by the addition of the active metals.

Based on the detected products, we constructed a tentative reaction pathway (Fig. 5). The latter was used to assemble a kinetic model. The corresponding kinetic parameters, based on the regression analysis, are shown in Table S2.

To confirm that no homogeneous reactions occurred, blank experiments were performed without any catalyst, where the substrates were glucose, GU and GA. Fig. S1 shows that no reaction occurred at 100 °C and 30 bar_g O_2, indicating that any oxidation that occurred was the result of the addition of the catalyst.

To better understand the reaction pathway, experiments were performed using GU, GLU and GA as the reactants with AuPt, at 100 °C and 30 bar_g O_2. Fig. 6a shows that when GU is used as the reactant, its oxidation to GLU is very slow, suggesting that the rate-determining step of the reaction is the second reaction in Fig. 5.

GA and TA were detected in the reaction mixture when the experiment was started with GLU, indicating that GA continues to react after its formation to TA and other C-C bond cleavage products (Fig. 6b). When the same experiment was performed with GA as the reactant (Fig. 6c), nearly all decomposition products were detected in the reaction mixture. Considering everything, it is obvious that GA is an intermediate and must be considered as such when reaction time and temperature are adjusted to achieve higher yields.

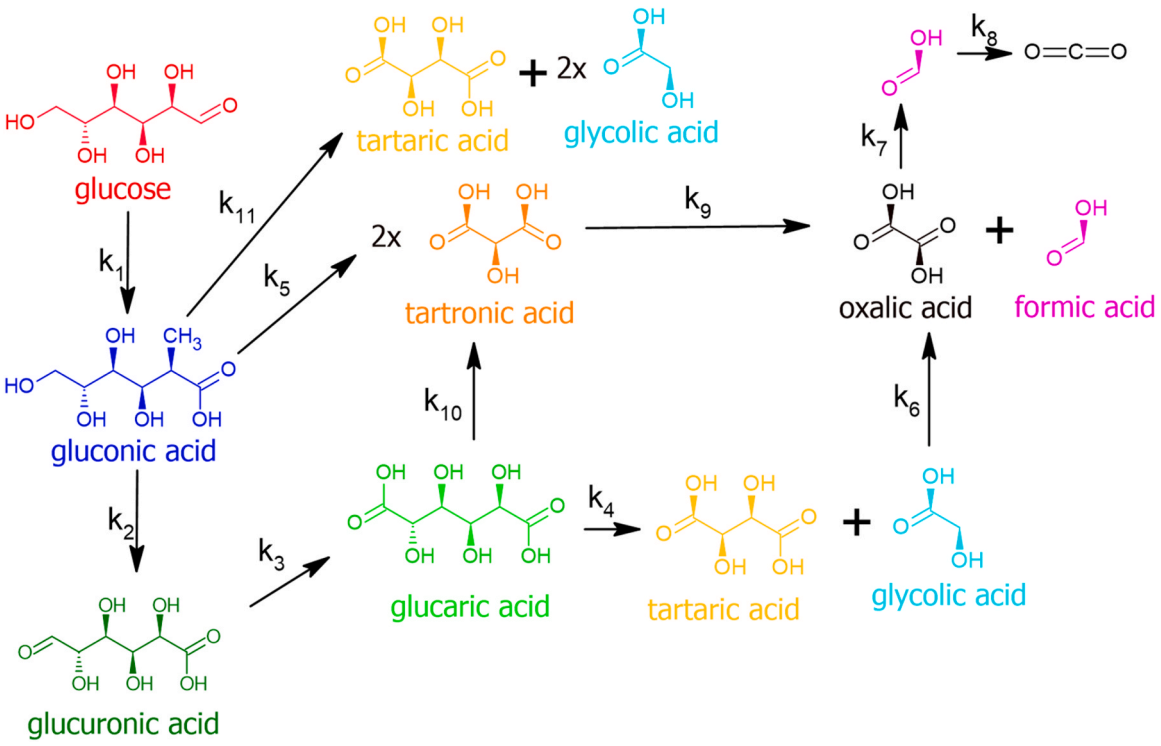

Fig. 5. Predicted reaction pathway for glucose oxidation. Each compound's colour matches the line colour in the concentration vs. time plots.

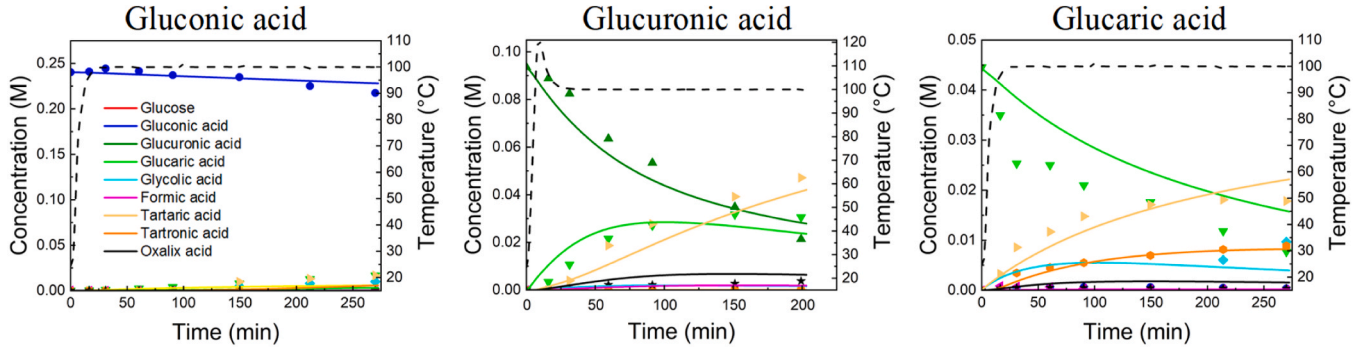

Fig. 6. Experiments with (a) GU, (b) GLU and (c) GA as reactants at 100 °C (—) and 30 bar_g O_2 on AuPt catalyst.

3.6. *Effect of temperature and pressure*

Initially, the experiments were performed with 50 mL of aqueous glucose and 16 bar_g O_2. In these experiments the final yield of GA is quite low (Fig. 7). We believe the poor conversion resulted from a low partial pressure of oxygen, which led to low concentration of dissolved O_2 and furthermore to low oxygen surface coverage. Consequently, a low concentration of GA in the final reaction mixture was detected. Moreover, the conversion of glucose was found to be higher for the AuCu and AuPt bimetallic catalysts.

Lower oxygen coverage on the surface affected the oxidation pathway of going beyond GU, since less O_2 is present on the catalyst's active sites. To increase the yield of GA, experiments were performed with higher oxygen pressure (30 bar_g) and a lower volume of aqueous glucose solution (40 mL). The molar ratio of glucose to active metal was the same in all experiments (Glu: metal = 40: 1). Fig. 8 compares the experiments performed with Au, AuCu and AuPt catalysts in the temperature range of 100–120 °C and 30 bar_g O_2.

An increase amount of O_2 partial pressure in the reactor led to an increase in the oxidation extent. At lower temperatures of 60 and 80 °C, the conversion of glucose and subsequently all other reactions are of low rate, as can be seen in Fig S1, where a clear difference is observed at the lower temperature. The conversion of glucose to GU is much lower when monometallic catalyst is used. When the temperature is raised to 100 °C, the conversion of GU is much faster. Compared to previously mentioned reaction conditions, AuPt catalyst exhibited a notably higher GA yield, peaking at 32% at 100 °C. When the temperature is raised to 120 °C, C-C bond cleavage starts to increase, which is evident by products such as TA, TO and GLY. The presence of both TA and TO, even before significant amounts of GA are formed, indicate that some C-C bond cleavage occurs even prior to GA formation. The calculated reaction rate constants and their corresponding activation energies are presented in Table S2.

The activation energy, calculated for the first reaction, the oxidation of aldehyde group of glucose, with monometallic Au, is 73 ± 2 kJ mol^{-1} which is higher, than for the same reaction with bimetallic AuCu and AuPt. The Ea_1 of bimetallic catalysts are 56 ± 3 kJ mol^{-1} and 50 ± 4 kJ mol^{-1} for AuCu and AuPt, respectively, which suggests that oxidation of terminal aldehyde group is more favourable. The reaction rate constant for the oxidation reaction of glucose to GU, calculated for

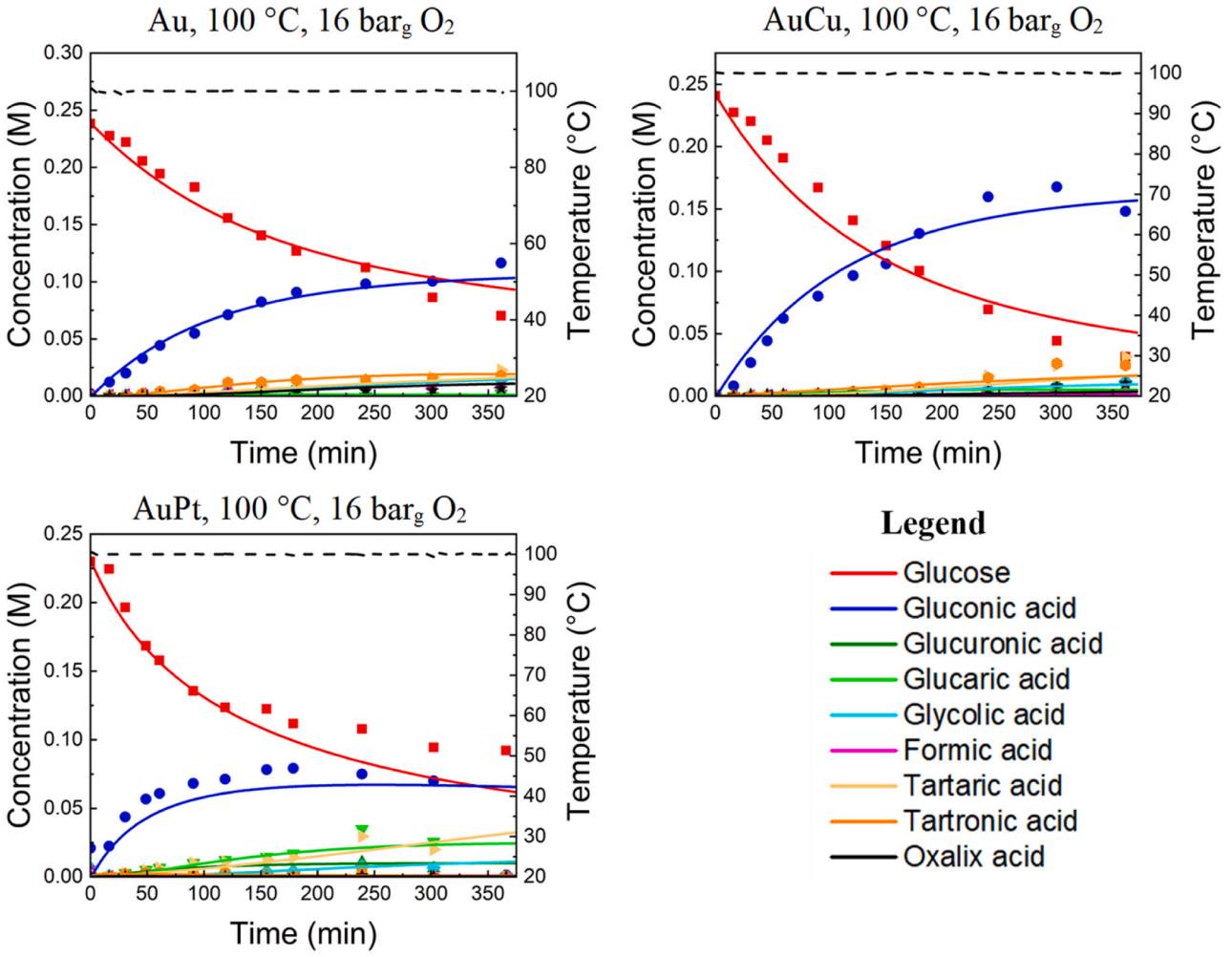

Fig. 7. Oxidation experiments performed at 100 °C (—) and 16 bar_g O_2.

AuPt was 1406 ± 23 min^{-1}, which was the highest among the catalysts tested, whereas the reaction rate constant on monometallic catalyst is 431 ± 23 min^{-1}. This is in accordance with DFT studies, presented below, where the activation barrier for the first reaction is higher on monometallic Au, compared to bimetallic counterparts.

An interesting indicator of each catalyst's potency is also the turnover frequency (TOF), presented in Table S3. The AuCu catalyst has the highest TOF value of 6.9E-03 $mol_{reactant}$ min^{-1} $g^{-1}_{active\ metal}$ for glucose conversion of all the materials we examined. This suggests, that if we replace half of golden atoms with copper atoms, whose molecular weight is more than 3-fold lower, the catalyst converts GLU molecules to GU with a noticeably higher frequency.

We postulate that the rate-limiting step is the second reaction, i.e. the oxidation of the terminal alcohol group of GU. Gupta *et al.*[80] made similar observation, when they studied hydroxymethyl furfural (HMF) transformation to furan dicarboxylic acid (FDCA) over gold catalyst, supported on hydrotalcite (HT). Their findings show that the aldehyde oxidation to carboxylic acid is relatively fast, as we have shown above, compared to the oxidation of terminal alcohol group, posed as the as the second reaction step. Our experiments show, that when comparing bimetallic catalysts, AuPt had enhanced activity for GU compared to AuCu and Au. Reaction rate constant was 75 ± 4 min^{-1}, which is 2-fold higher compared to AuCu and Au (Table S1). Interestingly, the activation energy, calculated for the second reaction, was 63 ± 3 kJ mol^{-1}, 49 ± 2 kJ mol^{-1} and 45 ± 1 kJ mol^{-1} on AuPt, AuCu and Au, respectively. This suggests not only that the oxidation of terminal alcohol is much faster on bimetallic AuPt catalyst, but also the fact that at higher temperatures, the reaction rate constant's value is rising even faster compared to the other two catalysts tested. Furthermore, connecting the dots with DFT, one can see that similar trend was observed there. The first reaction step **2a** in Table 1, the activation barriers on Au and AuCu catalysts are higher than for AuPt, supporting the microkinetic parameter evaluation.

The reaction rates for the third reaction step were 4928 ± 80 min^{-1}, 13022 ± 113 min^{-1} and 22319 ± 134 min^{-1} for Au, AuCu AuPt catalysts, respectively. Similarly, activation energy for this reaction is the highest for AuPt. Additionally, calculated DFT activation barriers for the third reaction (Table 1, step **2c**), where C-H bond scission occurs, are lower than for step **2a**. This implies, that once the terminal OH group is oxidized to an aldehyde, it is almost immediately further oxidized to a carboxylic acid. Moreover, considering the first reaction, where aldehyde group is oxidized to carboxylic acid, the trend is similar; AuPt catalyst has the best potency to perform such a reaction.

Since GU is the limiting step, and because Au catalyst still produces substantial amounts of GU, the question is what happens to GU, if it does not react further towards GA. For this reason, reactions 5 and 11, which present C-C scission reaction, affect the overall selectivity. From Table S1, Au seems to convert GU to by-products substantially faster than bimetallic catalysts. Reaction rate constants for reaction no. 5 are 5.2 ± 0.2 min^{-1}, 1.2 ± 0.1 min^{-1} and 0.73 ± 0.03 min^{-1}, for Au, AuCu and AuPt catalysts, respectively. The same conclusion can be made when reaction 11 is considered.

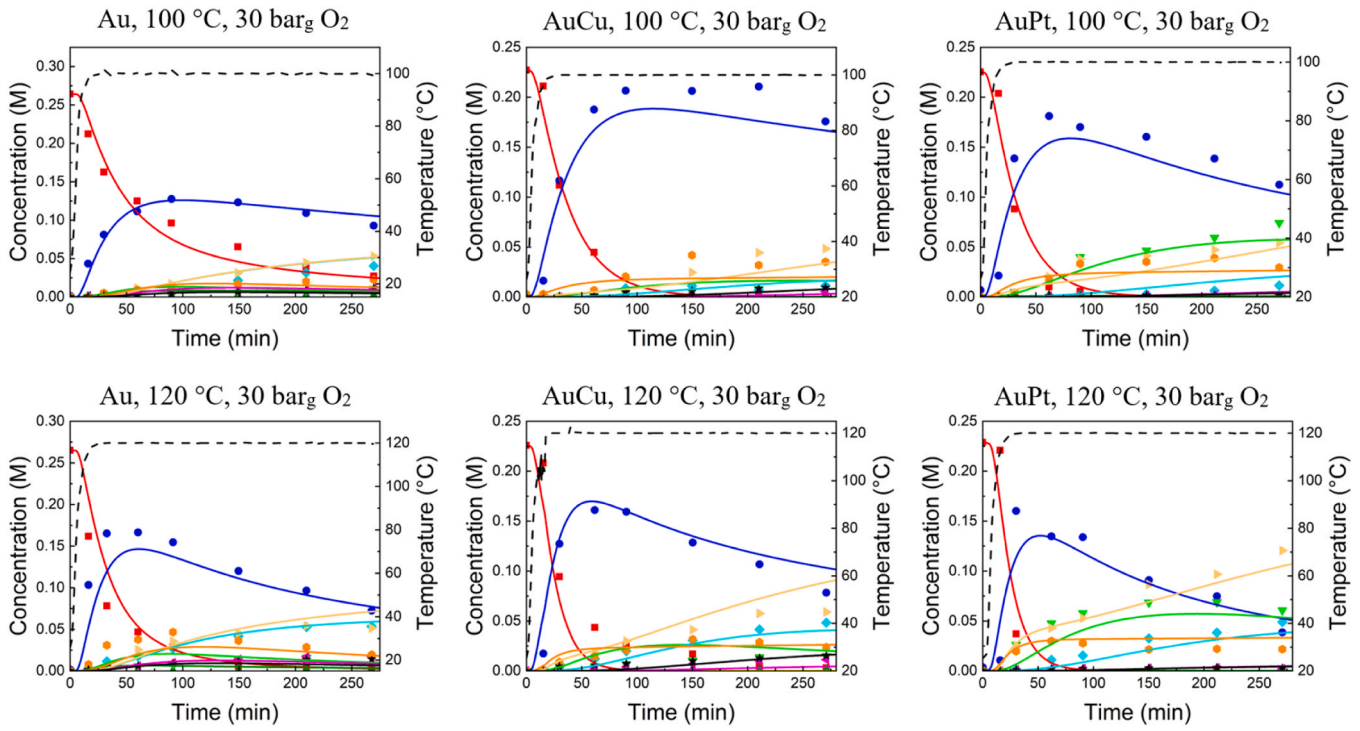

Fig. 8. Oxidation experiments conducted at temperatures of 100 and 120 °C (—) and 30 bar_g O_2.

Table 1
DFT-calculated activation barriers for the reaction steps in glucose oxidation. All values in eV.

	Au				Pt				Cu			
Step / oxidant species	none	O*	O_2 *	OH*	none	O*	O_2 *	OH*	none	O*	O_2 *	OH*
O_2 dissociation	1.76	n/a	n/a	n/a	0.56	n/a	n/a	n/a	0.15	n/a	n/a	n/a
Step 1a	1.66	0.24	0.21	0.22	0.74	0.57	0.50	0.34	1.06	0.19	0.22	0.43
Step 1b	0.11	n/a	n/a	n/a	0.06	n/a	n/a	n/a	0.34	n/a	n/a	n/a
Step 2a	1.85	0.37	0.08	0.28	0.91	0.25	0.05	0.17	1.68	0.26	0.03	0.36
Step 2b	0.52	0.38	0.43	0.45	0.31	0.47	0.58	0.47	0.81	0.82	1.12	1.24
Step 2c	1.38	0.77	0.74	0.66	0.37	0.78	0.81	0.30	0.93	0.85	0.75	0.95
Step 2d	n/a	0.39	n/a	0.46	n/a	0.25	n/a	0.61	n/a	0.68	n/a	1.05

Another crucial reaction for preserving GA is reaction no.4. Since Au produces barely any GA, the comparison has to be draw between AuCu and AuPt. The former's reaction constant rate is 38 ± 2 min^{-1}, which is 6-fold faster than with AuPt.

The formation of CO_2 is also an indicator of efficiency. The reaction rate constant for Au is 423 ± 10 min^{-1}, which is ~10 times higher than the reaction rate constants for the bimetallic catalysts. Fig. 9 shows the carbon balance (CB) for all catalysts. CB decreased for ~40% with Au catalyst. CB also decreased for AuCu catalyst for ~25%. In contrast to AuCu, CB decreased for AuPt catalyst for ~1%. Thus, the latter catalyst is far superior because the reaction rate is lower in the non-selective oxidation reactions.

In order to validate the parameters obtained by regression, the algorithm of the kinetic model was modified. Since the AuPt catalyst exhibited the highest yield, we decided to validate the model on this material. All reaction rate constants and corresponding activation energies were fixed, while time and temperature were introduced as input parameters of the regression function. The regression was stopped, when the highest yield of GA was reached at the end of the reaction time. In addition, the reaction time and temperature intervals (0.1 – 500 min and 60 – 340 °C, respectively) were investigated to find optimal conditions, for the highest yield of GA. Fig. 10 shows a 3D plot, where time and temperature represent the X and Y axes, respectively, while Z indicates the yield of GA in %.

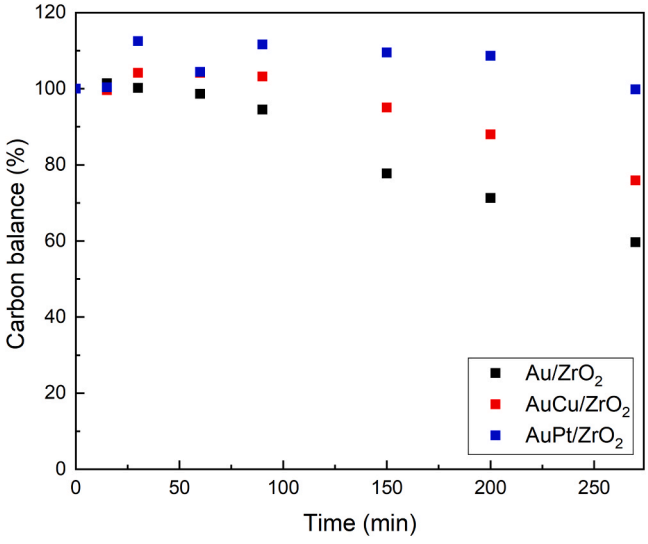

Fig. 9. Carbon balance for reactions at 120 °C, 40 mL of liquid phase and 30-bar gauge O_2.

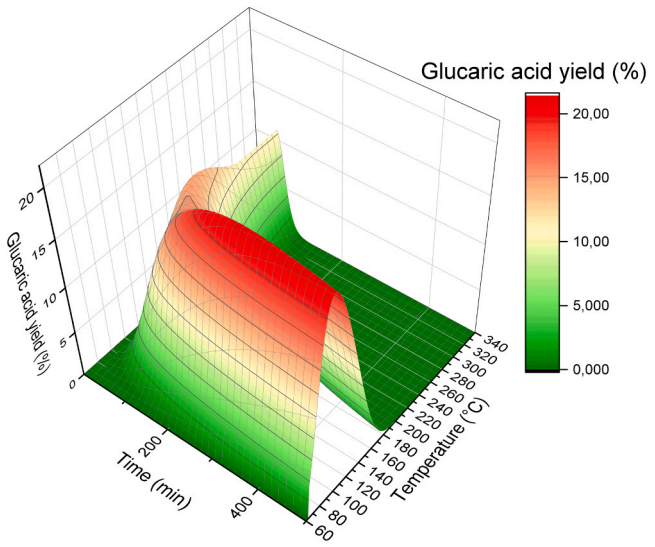

Fig. 10. GA yield predicted by the model at whole relevant reaction time (0.1 – 500 min) and temperature window (60–340 °C).

It can be seen that the "sweet spot" is at 118 °C and 170 min. When the reaction time is extended, the yield of GA slowly decreases. Therefore, the predicted temperature and time were 118 °C and 170 min, respectively. Then, the experiment was performed with the predicted time and temperature and later compared with the values predicted by the model. The results are shown in Fig. 11.

The predicted profile lines of the concentrations of glucose, GA, TO, OX and FA agree well with the experimental data. However, there is still room for improvement of the model, because GU, TA and GLY do not follow the profile line predicted by the model. Further experimental and modelling studies should be conducted, to elucidate the reaction pathway in more detail and improve the ability of the model to predict the concentrations of all compounds during the reaction time.

3.7. First-principles insight

To better understand the different activity of the tested catalytic materials, the interaction of different metal surfaces Au (111) (schematically shown in Fig. 12), Cu (111) and Pt (111) with oxygen, glucose and GU was studied. For oxygen availability, AuCu and AuPt were also modelled, while glucose and GU oxidation was studied on pristine surfaces only (because of nano-sized crystallites present in the catalyst).

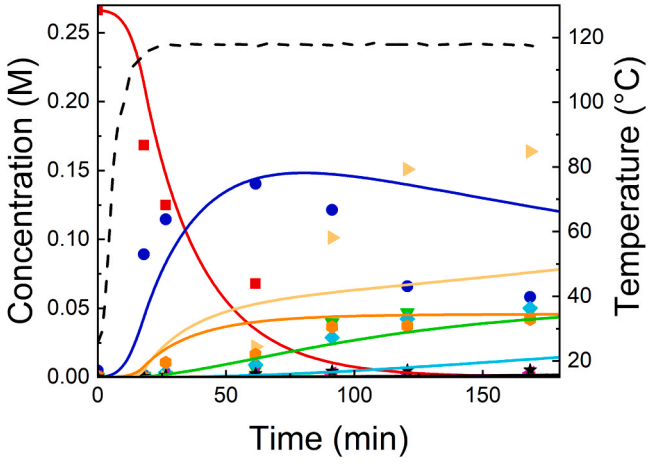

Fig. 11. Validation experiment at model-based optimized reaction conditions to maximize the yield of GA acid using AuPt catalyst: 118 °C (—), 30 bar_g O_2 and reaction time of 170 min.

Au, Cu and Pt are well known for their differences in oxophilicity [81]. The binding energy for atomic oxygen on Au, Pt, and Cu is − 0.22 eV, − 1.33 eV and − 1.74 eV, respectively. As shown by Frey, the formation energy of an oxygen adatom is a monotonously increasing positive function of surface concentration for Au. For Pt, is has a minimum around 0.7 mL but is positive in the whole coverage range. For Cu, it is negative (favourable) between 0.25 mL and 0.65 mL. This means that, theoretically, under all reaction conditions, there will be most active oxygen available on Cu, less on Pt and very little on Au.

To correlate the experimentally observed reaction rates with the oxophilicity of different metals, glucose oxidation to GU was modelled. Assuming a pyranose (six-member ring) structure, adsorption energies of glucose on Au (111), Pt (111) and Cu (111) are found to be very similar: 1.31 eV, 1.44 eV and 1.59 eV. For GU, these values are 1.29 eV, 1.33 eV and 1.30 eV. Thus, we deem it highly unlikely that the difference in the performance of the tested catalysts is brought about by this phenomenon.

Instead, different oxophilicity of the metals seems to play a crucial role. We calculated the adsorption values for O_2 on Au, Pt and Cu as − 0.14 eV, − 0.59 eV and − 0.49 eV, respectively. On intermetallics, the values are − 0.46 eV on AuCu and − 0.57 eV on AuPt, as O_2 binds to Cu and Pt atoms, respectively. However, the barriers and reaction energies (in parenthesis) for O_2 dissociation are 1.76 eV (+0.48 eV), 0.56 eV (−1.28 eV), 0.15 eV (−1.99 eV), 0.63 eV (−1.11 eV) and 0.77 eV (−0.83 eV) on Au, Pt, Cu, AuCu, and AuPt, respectively.

This paints a rather straightforward picture. There is very little O_2 and virtually no O* on Au, while the addition of Pt adds mostly O_2 and some O, and Cu activates oxygen to O* . When Au is combined with Cu or Pt, more oxygen is available, while the favourable reaction energetics of glucose oxidation is retained. This corroborates the experimental findings, which we further discuss on in the next section.

To evaluate the consequences of different oxygen environments on different catalysts, we calculated the reaction parameters for the two-step glucose oxidation to GU and four-step oxidation of GU to GLU, as presented in Fig. 13. Pristine metals were chosen because of limited miscibility of Au with Cu and Pt and because the trends on individual metals are of interest.

In aqueous solutions, such as our reaction system, glucose is predominantly present as a six-membered ring (glucopyranose) [82]. In the first reaction, the terminal aldehyde group is oxidised to the carboxyl group, yielding GU [83]. Since glucopyranose is formed by a reaction of the aldehyde group with 5-OH, the ensuing GU is formed in the lactone form (glucono delta-lactone). This is achieved by first removing the hydroxyl hydrogen atom, followed by the cleavage of the C-H bond.

For the sake of completeness, we investigate all four scenarios for each elementary step. Where a hydrogen atom is cleaved off, this can happen in a non-assisted way, or with reactive oxygen species on the surface (O*, O_2 * or OH*). The barriers for the elementary steps are given in Table 1. It should be noted, however, that not all of them are abundant on all catalysts. For instance, on Au, little O* is available.

A clear general trend emerges. The rate determining step is the cleavage of the first hydrogen atom. The barriers for spontaneous hydrogen abstraction are higher (1.66 eV, 1.06 eV and 0.74 eV on Au, Cu and Pt, respectively) than with oxygen reactive species (~0.2 eV on Au, 0.2–0.43 eV on Cu, 0.3–0.5 eV on Pt). The second elementary step, i.e. the cleavage of the C-H bond, occurs without a participating oxygen species (barriers of 0.11 eV, 0.34 eV, 0.06 eV on Au, Cu, Pt respectively).

In the second transformation, GU is oxidised to GA via four elementary steps. The rate determining step varies based on the oxidant species encountered. Generally, the barriers are highest on Au and lowest on Pt. For instance, Step 2a with O* has barriers of 0.37 eV, 0.26 eV and 0.25 eV on Au, Cu, and Pt, respectively. The last elementary step requires a presence of O* or OH* to complete the oxidation of the aldehyde group to GA. See Table 1 for all the values.

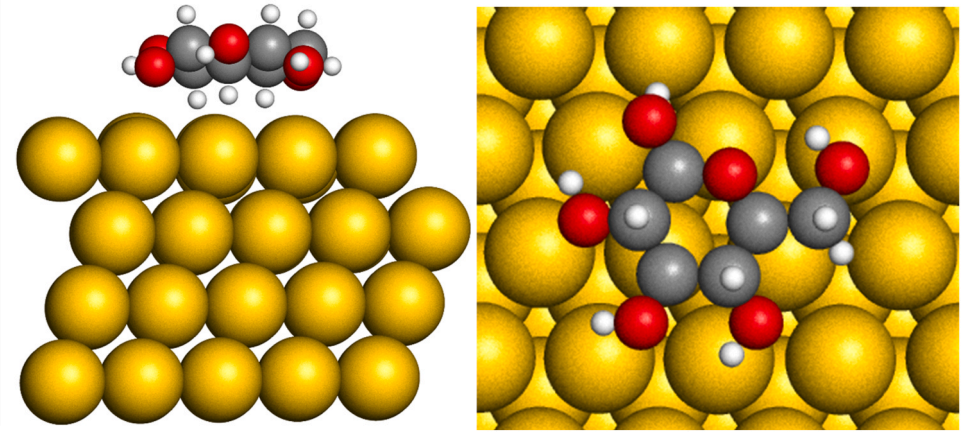

Fig. 12. (left) A perspective and (right) top view of glucose adsorbed on Au (111).

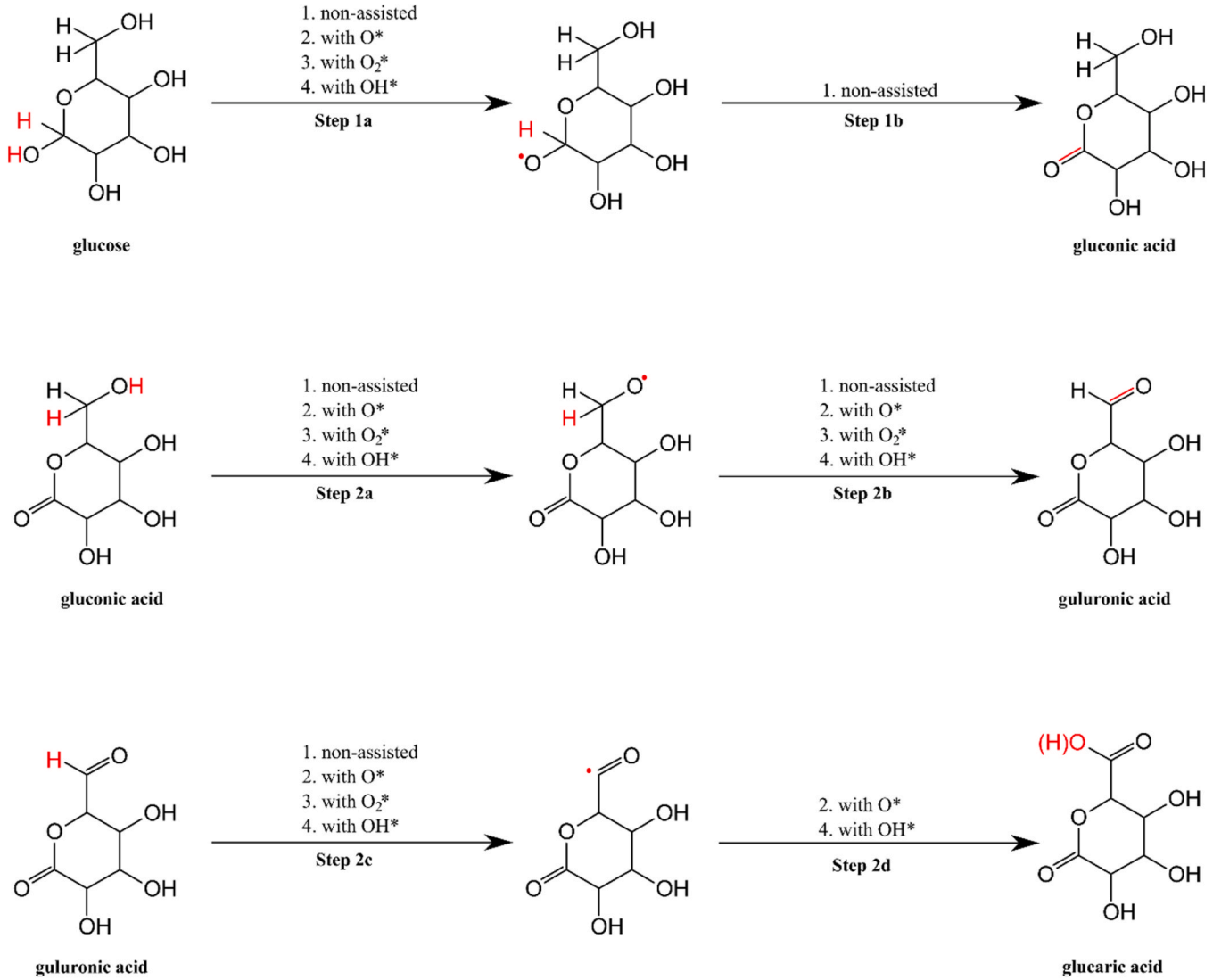

Fig. 13. Elementary reaction mechanism of the oxidation of glucose via GU to GA with different oxygen species present, as studied by DFT.

Based on the analysis of the reaction barriers, Pt would stand out as a superior catalyst compared to Au and Cu. However, experiments show that pure Pt is ill-suited for the production of GA as it steers the reaction towards the undesired short-chain products. Computational data explains this further. Not only are oxygen reactive species on Pt present in excess, C-C bond cleavage is thermodynamically favourable. For the C3-C4 bond cleavage (see Fig. 14) in GU, the energy of reaction is + 1.40 eV, + 1.27 eV and −0.06 eV on Au, Cu, and Pt, respectively. This

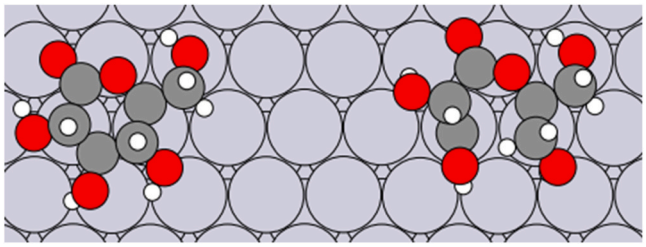

Fig. 14. Cleavage of C3-C4 bond in GU, shown on Pt (111).

means that Pt would favour the decomposition of C6 derivatives of glucose to smaller molecules. The shortcomings of pure Pt are alleviated by using bimetallic catalysts. For AuCu and AuPt, when modelled as perfect alloys, the energy of reaction for this step is + 1.40 eV and + 1.10 eV, respectively, showing they do not cleave the C-C bonds.

With the DFT analysis, the suitability of the microkinetic approach is explained. As shown in Fig. 5, the microkinetic model only accounts for stable intermediates, which are experimentally measurable. This lumped approach is warranted because the elementary steps, forming individual lumped transformation, have very different activation barriers. This means that one is treated as a rate-determining step – featuring the microkinetic model – while the rest are fast and pseudo-stationary. A detailed inspection of Table 1 shows that the O-H activation initiates the oxidation of glucose, which is followed by a quick C-H cleavage. For gluconic acid and guluronic acid, however, the C-H bond activation is actually slower (provided an oxidative species is present on the surface).

4. Discussion

The results of XPS, TEM and XRD confirmed the formation of alloys in the studied bimetallic catalysts. Moreover, the results show that the applied synthesis technique produces metallic nanoparticles. In both the mixed AuPt and AuCu samples, a weak diffuse diffraction peak at ~38°2θ, with much lower intensity than in the pure Au-loaded sample, indicates the presence of nano-sized Au crystallites coexisting with the mixed AuPt and AuCu phases. The percentage of the pure gold phase in the bimetallic materials is negligible. However, no separate Pt or Cu diffractions were observed, which would indicate separate deposition of the metals. It is worth noting that we sporadically detected a weak Au diffraction peak, possibly due to splitting of the diffraction peak, indicating initial phase separation and dealloying, or representing a pure Au residue that deposited separately and not as part of the AuPt alloy. These results correlate well with the observation of a weak Au (111) diffraction peak in the AuPt sample. The increase in oxygen adsorption observed when Cu and Pt metals are introduced into the Au substrate indicates a significant improvement in the surface coverage of oxygen on the bimetallic catalysts when operated under optimised reaction conditions. This observation is consistent with the results of density functional theory calculations (DFT), which indicate a reduced activation energy for the dissociative adsorption of oxygen, especially on Pt and Cu surfaces. Furthermore, these results are confirmed by existing literature, e.g. Gottfried et al. who found that molecular oxygen (O_2) does not dissociate on Au surfaces.[84] Under the aforementioned reaction conditions, it can be seen that the Au surface remains predominantly unaffected, while Pt alloys are enveloped by oxygen species referred to as O_2* and some O*, and Cu predominantly accumulates O*. These differences in surface composition lead to profound differences in catalytic activity.

Our DFT calculations showed that the activation barriers for the O-H and C-H cleavages, necessary for the oxidation of glucose to GU and to GA, are highest on Au and lowest on Pt. However, when fewer active oxygen species are available, the reaction is slower and more selective, which is the case for Au. Cu and Pt exhibit a higher surface concentration of active oxygen species, which is the reason for their markedly different activity. However, an excessive concentration of nucleophilic O* species facilitates over-oxidation, including the undesired C-C bond cleavage, which is detrimental for yields. This is especially pronounced on pure Pt, where C-C bond cleavage is slightly exothermic, while on Au and Cu it is endothermic. The results also agree well with the work of Rautiainen et al. [85] who found that Au has the ability to oxidise guluronic acid to GA. Table 1 shows that the barrier in Step 2a (oxidation of GU) is higher than in Step 2c (oxidation of GLU). Hence, poor performance of pure Au is due to its inability to convert GU. On the other hand, should glucuronic acid be present, it is readily oxidised further.

The easier oxygen activation is favoured by the shift of the electronic structure in the bimetallic catalysts and promotes the higher activity of the synthesised materials. However, this promoting effect must be fine-tuned so as not to accelerate the overoxidation of GA. This is indicated by the XPS results for the AuCu catalyst, where the Au 4 f peak shifts to higher binding energies. We believe that this shift in binding energy favours stronger adsorption of electron-rich (-COOH) species of the products, leading to C-C bond cleavage or decarboxylation and thus lower selectivity. The experimentally observed oxygen species on the metals used support the proposed mode of action [86]. The weak binding of O_2 on Au surfaces, where no activated oxygen species were observed, indicates negligible charge transfer. On the other hand, several activated oxygen species are observed on Pt and Cu surfaces. Hyman and Medlin [87] found that a combination of Au with Pt or Cu results in a weak O_2 binding, but very strong O binding. We believe that the modified charge transfer not only contributes to a stronger binding, but in the case of Cu, also generates stronger (more electrophilic) oxygen species that cause further oxidation of GA.

From the experimental data and the model in Fig. 8, we can conclude, that our assumptions regarding the oxidation activity of each material correlate quite well. The bimetallic materials clearly produce more GU than the monometallic counterpart does. The calculated activation energy is two-fold higher, which compares well to the results of DFT. On the other hand, the turnover frequencies and activation energies, for the monometallic catalyst, indicate that whatever GA is formed, it is then quickly converted further to shorter chain products, and finally to carbon dioxide. We believe a low oxygen surface coverage of the latter material causes this, as it enables the adsorption of oxygenates. The carbon balance presented in Fig. 9, where a significant drop is evident when Au and AuCu catalysts were used, also indicates this. In addition, we conducted recycle tests where we reused the same material for 3 consecutive oxidation tests (Fig. S4). Only the bimetallic catalysts were used, as there is a lot of data in the literature showing that monometallic Au-based catalysts are completely stable. We stopped the reaction when we expected a conversion of about 50% so that we could detect minimal deviations that would indicate deactivation of the catalyst. No such deviations were observed and the bimetallic materials remained quite stable during the three cycles.

Comparing our results with the few literature results, it can be seen that large number of parameters influence the overall yield of GA. The comparison is presented in Table S4. The most important process parameters are reaction temperature, oxygen partial pressure, molar ratio of glucose and metal (mol/mol) and reaction time. Derrien et al. [83] performed reaction with AuPt/ZrO_2 catalyst, prepared with different deposition precipitation procedure and reported a 50% GA yield at 100 °C and 50 bar_g O_2 pressure. Lee et al. [88] reported a 74% yield of GA at 80 °C, 13.8 bar_g O_2 pressure, a glucose to metal ratio of 54 and 10 h reaction time. The catalyst used in this case was Pt/C. Furthermore, we added a comparison table in SI (Table S3), for easier comparison. Compared to all these different catalysts and process parameters, our reaction yield was highest with the bimetallic AuPt/ZrO_2 catalyst. The GA yield was 32% at 100 °C, 30 bar_g O_2 pressure and a molar ratio of 40. Contrary to several other studies, our reaction time was quite short (3.3 h), and the initial glucose concentration was relatively high (0.25 M).

Conclusion

DFT calculations corroborated that the difference in performance of Au, AuPt and AuCu. The latter can be attributed to their differing oxophilicity. The reaction proceeds differently because there is little available oxygen on Au, while Pt supplies O_2 * and O* , and Cu provides ample O* . Both oxygen species increase the reaction rate but can lead to overoxidation if present in excessive amounts, which is modulated by catalyst composition. For the sake of completeness, it was found that OH* behaves similarly. For instance, on Au the activation barrier for glucose oxidation is 1.40 eV, which drops precipitously to < 0.3 eV when O_2 * or O* is available. This hints that the reaction is governed by the rate of oxygen adsorption and decomposition, which is caused by a changed oxophilicity of the surface (electronic effect) and not the lattice expansion effect since pure Au, Cu and Pd have very different lattice constant but enable similar energetics *provided* that the same active oxygen species were present.

Connecting the dots with DFT, microkinetic study correlates well with the ab initio calculations. Oxidation of glucose to GU by Au is hindered by the weak ability of oxygen utilization. While bimetallic AuPt provides both oxygen species O_2 * and O* and has the highest selectivity among the three, AuCu seems to be too potent for selective oxidation towards GA. All of the theoretical results were further substantiated by experimental data.

To the best of our knowledge, this is one of few studies encompassing catalyst synthesis, characterization, DFT study and microkinetic modelling of the experimental results. We believe this study to be a good foundation stone for future research in the quest to introduce biomass valorisation and higher engagement in the field of circular economy.

CRediT authorship contribution statement

The contributions of the authors in this work were as follows: Žan Lavrič played a multi-faceted role encompassing Methodology, Validation, Investigation, Writing – original draft, Writing – review & editing. Janvit Teržan contributed significantly to Conceptualization, Methodology, Validation, Investigation, Writing – original draft, Writing – review & editing, and provided Supervision. Ana Kroflič concentrated on the Methodology aspect of the research. Janez Zavašnik was involved in Methodology and Investigation. Joanna Elżbieta Olszówka took on the responsibilities of Writing – original draft and Writing – review & editing. Štefan Vajda was instrumental in Funding acquisition. Matej Huš contributed extensively to Conceptualization, Methodology, Validation, and Funding acquisition. Miha Grilc played a role in Methodology and Supervision. Blaž Likozar contributed to Conceptualization, Methodology, Validation, and Funding acquisition. Each author's unique expertise and efforts combined to make this research possible.

Declaration of Competing Interest

The authors declare that they have no known competing financial interests or personal relationships that could have appeared to influence the work reported in this paper.

Data Availability

Data will be made available on request.

Acknowledgements

The work of authors J. E. Olszowka and S. Vajda was supported by the Grant Agency of the Czech Republic in the frame of the Lead Agency Project ARRS, Slovenian Research Agency, Grant No. 21-48595L. M.H. appreciates the Slovenian Research Agency project funding J2-4424, infrastructure funding I0-0039 and core funding P2-0421. B.L. appreciates the Slovenian Research Agency core funding P2-0152. J.T., M.G., and B.L. appreciate the Slovenian Research Agency funding J7-4638, J1-3028, J1-3020, N2-0242, NC-0024, and J2-2492. The authors gratefully acknowledge the HPC RIVR consortium (www.hpc-rivr.si) and EuroHPC JU (eurohpc-ju.europa.eu) for funding this research by providing computing resources of the HPC system Vega at the Institute of Information Science (www.izum.si).

Appendix A. Supporting information

Supplementary data associated with this article can be found in the online version at doi:10.1016/j.apcatb.2023.123455.

References

[1] Z. Zhang, J. Song, B. Han, Catalytic transformation of lignocellulose into chemicals and fuel products in ionic liquids, Chem. Rev. 117 (2017) 6834–6880, https://doi.org/10.1021/acs.chemrev.6b00457.
[2] B.M. Upton, A.M. Kasko, Strategies for the conversion of lignin to high-value polymeric materials: review and perspective, Chem. Rev. 116 (2016) 2275–2306, https://doi.org/10.1021/acs.chemrev.5b00345.
[3] S.L.Y. Lo, B.S. How, W.D. Leong, S.Y. Teng, M.A. Rhamdhani, J. Sunarso, Techno-economic analysis for biomass supply chain: a state-of-the-art review, Renew. Sustain. Energy Rev. 135 (2021), 110164, https://doi.org/10.1016/j.rser.2020.110164.
[4] P.L. Arias, J.A. Cecilia, I. Gandarias, J. Iglesias, M. López Granados, R. Mariscal, G. Morales, R. Moreno-Tost, P. Maireles-Torres, Oxidation of lignocellulosic platform molecules to value-added chemicals using heterogeneous catalytic technologies, Catal. Sci. Technol. 10 (2020) 2721–2757, https://doi.org/10.1039/D0CY00240B.
[5] C.O. Tuck, E. Pérez, I.T. Horváth, R.A. Sheldon, M. Poliakoff, Valorization of biomass: deriving more value from waste, Science 337 (2012) (1979) 695–699, https://doi.org/10.1126/science.1218930.
[6] R. Gérardy, D.P. Debecker, J. Estager, P. Luis, J.-C.M. Monbaliu, Continuous flow upgrading of selected C_2–C_6 platform chemicals derived from biomass, Chem. Rev. 120 (2020) 7219–7347, https://doi.org/10.1021/acs.chemrev.9b00846.
[7] M. Besson, P. Gallezot, C. Pinel, Conversion of biomass into chemicals over metal catalysts, Chem. Rev. 114 (2014) 1827–1870, https://doi.org/10.1021/cr4002269.
[8] Z. Walaszek, Potential use of d-glucaric acid derivatives in cancer prevention, Cancer Lett. 54 (1990) 1–8, https://doi.org/10.1016/0304-3835(90)90083-A.
[9] Z. Walaszek, J. Szemraj, M. Hanausek, A.K. Adams, U. Sherman, d-Glucaric acid content of various fruits and vegetables and cholesterol-lowering effects of dietary d-glucarate in the rat, Nutr. Res. 16 (1996) 673–681, https://doi.org/10.1016/0271-5317(96)00045-0.
[10] J.B.J.H. van Duuren, B. Brehmer, A.E. Mars, G. Eggink, V.A.P.M. dos Santos, J.P. M. Sanders, A limited LCA of bio-adipic acid: Manufacturing the nylon-6,6 precursor adipic acid using the benzoic acid degradation pathway from different feedstocks, Biotechnol. Bioeng. 108 (2011) 1298–1306, https://doi.org/10.1002/bit.23074.
[11] J. Singh, K.P. Gupta, Calcium glucarate prevents tumor formation in mouse skin, Biomed. Environ. Sci. 16 (2003) 9–16.
[12] D.R. Okada, G. Johnson, Z. Liu, S.D. Hocherman, B.-A. Khaw, R.D. Okada, Early detection of infarct in reperfused canine myocardium using 99mTc-glucarate, J. Nucl. Med 45 (2004) 655–664.
[13] B. Hočevar, A. Prašnikar, M. Huš, M. Grilc, B. Likozar, H_2 -free re-based catalytic dehydroxylation of aldaric acid to muconic and adipic acid esters, Angew. Chem. Int. Ed. 60 (2021) 1244–1253, https://doi.org/10.1002/anie.202010035.
[14] T.N. Smith, K. Hash, C.-L. Davey, H. Mills, H. Williams, D.E. Kiely, Modifications in the nitric acid oxidation of d-glucose, Carbohydr. Res 350 (2012) 6–13, https://doi.org/10.1016/j.carres.2011.12.024.
[15] C.L. Mehltretter, C.E. Rist, Sugar oxidation, saccharic and oxalic acids by the nitric acid oxidation of dextrose, J. Agric. Food Chem. 1 (1953) 779–783, https://doi.org/10.1021/jf60012a005.
[16] J. Yin, Q. Zhang, C. Yang, B. Zhang, K. Deng, Highly selective oxidation of glucose to gluconic acid and glucaric acid in water catalyzed by an efficient synergistic photocatalytic system, Catal. Sci. Technol. 10 (2020) 2231–2241, https://doi.org/10.1039/C9CY02393C.
[17] D. Bin, H. Wang, J. Li, H. Wang, Z. Yin, J. Kang, B. He, Z. Li, Controllable oxidation of glucose to gluconic acid and glucaric acid using an electrocatalytic reactor, Electro Acta 130 (2014) 170–178, https://doi.org/10.1016/j.electacta.2014.02.128.
[18] X. Bai, Q. Hou, H. Qian, Y. Nie, T. Xia, R. Lai, G. Yu, M. Laiq Ur Rehman, H. Xie, M. Ju, Selective oxidation of glucose to gluconic acid and glucaric acid with chlorin e6 modified carbon nitride as metal-free photocatalyst, Appl. Catal. B. 303 (2022), 120895, https://doi.org/10.1016/j.apcatb.2021.120895.
[19] T.S. Moon, S.-H. Yoon, A.M. Lanza, J.D. Roy-Mayhew, K.L.J. Prather, Production of glucaric acid from a synthetic pathway in recombinant *Escherichia coli*, Appl. Environ. Microbiol 75 (2009) 589–595, https://doi.org/10.1128/AEM.00973-08.
[20] Tetsuya Ito, Hiroki Tadokoro, Hisaharu Masaki, Katsuhiko Mikuni, Hiromi Murakami, Taro Kiso, Takaaki Kiryu, D-glucaric acid-producing bacterium, and method for manufacturing d-glucaric acid, n.d. https://patents.google.com/patent/EP2857496A1/en (accessed December 22, 2022).

[21] I.M.B. Reizman, A.R. Stenger, C.R. Reisch, A. Gupta, N.C. Connors, K.L.J. Prather, Improvement of glucaric acid production in E. coli via dynamic control of metabolic fluxes, Metab. Eng. Commun. 2 (2015) 109–116, https://doi.org/10.1016/j.meteno.2015.09.002.
[22] P. Punthong, S. Visitsatthawong, L. Chuaboon, P. Chaiyen, T. Wongnate, Chemo-enzymatic synthesis of sugar acid by pyranose 2-oxidase, Mol. Catal. 533 (2022), 112753, https://doi.org/10.1016/j.mcat.2022.112753.
[23] G. Kovačević, R.G.A. Elgahwash, M. Blažić, N. Pantić, O. Prodanović, A.M. Balaž, R. Prodanović, Production of fructose and gluconic acid from sucrose with cross-linked yeast cell walls expressing glucose oxidase on the surface, Mol. Catal. 522 (2022), 112215, https://doi.org/10.1016/j.mcat.2022.112215.
[24] J.-F. Thaburet, N. Merbouh, M. Ibert, F. Marsais, G. Queguiner, TEMPO-mediated oxidation of maltodextrins and d-glucose: effect of pH on the selectivity and sequestering ability of the resulting polycarboxylates, Carbohydr. Res 330 (2001) 21–29, https://doi.org/10.1016/S0008-6215(00)00263-9.
[25] M. Ibert, F. Marsais, N. Merbouh, C. Brückner, Determination of the side-products formed during the nitroxide-mediated bleach oxidation of glucose to glucaric acid, Carbohydr. Res. 337 (2002) 1059–1063, https://doi.org/10.1016/S0008-6215(02)00072-1.
[26] N. Merbouh, J.M. Bobbitt, C. Brueckner, ChemInform abstract: 4-AcNH-TEMPO-catalyzed oxidation of aldoses to aldaric acids using chlorine or bromine as terminal oxidants (no-no), ChemInform 33 (2010), https://doi.org/10.1002/chin.200241196.
[27] P. Pan, M. Li, Y. Liu, Y. Feng, X. Li, Selective oxidation of 5-hydroxymethylfurfural into 2,5-diformylfuran by TEMPO-assisted magnetic Fe3O4@SiO2@mSiO2-NH2-Cu(II) catalytic system, Mol. Catal. 530 (2022), 112622, https://doi.org/10.1016/j.mcat.2022.112622.
[28] Q.N.B. Nguyen, H.B. Phan, T.H. Nguyen, V.T.C. Doan, L.B. Nguyen, H.T. Nguyen, P.H. Tran, Direct and low-cost transformation of glucose to 2,5-diformylfuran by AlCl3·6H2O, sulfur, and dimethyl sulfoxide, Mol. Catal. 530 (2022), 112588, https://doi.org/10.1016/j.mcat.2022.112588.
[29] X. Yu, Z. Zhao, L. Zhu, S. Tan, W. Fu, L. Wang, Y. An, Aerobic oxidative cleavage and esterification of C C bonds catalyzed by iron-based nanocatalyst, Mol. Catal. 519 (2022), 112152, https://doi.org/10.1016/j.mcat.2022.112152.
[30] X. Tan, W. Deng, M. Liu, Q. Zhang, Y. Wang, Carbon nanotube-supported gold nanoparticles as efficient catalysts for selective oxidation of cellobiose into gluconic acid in aqueous medium, Chem. Commun. (2009) 7179, https://doi.org/10.1039/b917224f.
[31] I. Witońska, M. Frajtak, S. Karski, Selective oxidation of glucose to gluconic acid over Pd–Te supported catalysts, Appl. Catal. A Gen. 401 (2011) 73–82, https://doi.org/10.1016/j.apcata.2011.04.046.
[32] H. Sakurai, K. Koga, M. Kiuchi, Gold nanoparticles deposited on Amberlyst-15: Metal–acid bifunctional catalyst for cellobiose conversion to gluconic acid, Catal. Today 251 (2015) 96–102, https://doi.org/10.1016/j.cattod.2014.11.004.
[33] Y. Wang, S. van de Vyver, K.K. Sharma, Y. Román-Leshkov, Insights into the stability of gold nanoparticles supported on metal oxides for the base-free oxidation of glucose to gluconic acid, Green. Chem. 16 (2014) 719–726, https://doi.org/10.1039/C3GC41362D.
[34] M. COMOTTI, C. DELLAPINA, E. FALLETTA, M. ROSSI, Is the biochemical route always advantageous? The case of glucose oxidation, J. Catal. 244 (2006) 122–125, https://doi.org/10.1016/j.jcat.2006.07.036.
[35] A. Mirescu, U. Prüße, A new environmental friendly method for the preparation of sugar acids via catalytic oxidation on gold catalysts, Appl. Catal. B. 70 (2007) 644–652, https://doi.org/10.1016/j.apcatb.2006.01.017.
[36] B.T. Kusema, B.C. Campo, O.A. Simakova, A.-R. Leino, K. Kordás, P. Mäki-Arvela, T. Salmi, D.Y. Murzin, Selective Oxidation of D-Galactose over Gold Catalysts, ChemCatChem 3 (2011) 1789–1798, https://doi.org/10.1002/cctc.201100183.
[37] P.J. Miedziak, H. Alshammari, S.A. Kondrat, T.J. Clarke, T.E. Davies, M. Morad, D. J. Morgan, D.J. Willock, D.W. Knight, S.H. Taylor, G.J. Hutchings, Base-free glucose oxidation using air with supported gold catalysts, Green. Chem. 16 (2014) 3132–3141, https://doi.org/10.1039/C4GC00087K.
[38] Y. Cao, X. Liu, S. Iqbal, P.J. Miedziak, J.K. Edwards, R.D. Armstrong, D.J. Morgan, J. Wang, G.J. Hutchings, Base-free oxidation of glucose to gluconic acid using supported gold catalysts, Catal. Sci. Technol. 6 (2016) 107–117, https://doi.org/10.1039/C5CY00732A.
[39] S. Rautiainen, P. Lehtinen, M. Vehkamäki, K. Niemelä, M. Kemell, M. Heikkilä, T. Repo, Microwave-assisted base-free oxidation of glucose on gold nanoparticle catalysts, Catal. Commun. 74 (2016) 115–118, https://doi.org/10.1016/j.catcom.2015.11.014.
[40] D.M. Alonso, S.G. Wettstein, J.A. Dumesic, Bimetallic catalysts for upgrading of biomass to fuels and chemicals, Chem. Soc. Rev. 41 (2012) 8075, https://doi.org/10.1039/c2cs35188a.
[41] X. Jin, M. Zhao, J. Shen, W. Yan, L. He, P.S. Thapa, S. Ren, B. Subramaniam, R. v Chaudhari, Exceptional performance of bimetallic Pt1Cu3/TiO2 nanocatalysts for oxidation of gluconic acid and glucose with O2 to glucaric acid, J. Catal. 330 (2015) 323–329, https://doi.org/10.1016/j.jcat.2015.05.018.
[42] Vincent J. Murphy, James Shoemaker, Guang Zhu, Raymond Archer, George Frederick Salem, Eric L. Dias, Catalyst comprising platinum and gold nano - particles and its use for oxidation of glucose and preparation method of such a catalyst, n.d. ⟨https://patents.google.com/patent/WO2011155964A1/en⟩ (accessed December 22, 2022).
[43] J. Lee, B. Saha, D.G. Vlachos, Pt catalysts for efficient aerobic oxidation of glucose to glucaric acid in water, Green. Chem. 18 (2016) 3815–3822, https://doi.org/10.1039/C6GC00460A.
[44] G. Diamond, V. Murphy, T. Boussie, Application of High Throughput Experimentation to the Production of Commodity Chemicals from Renewable Feedstocks, in: Modern Applications of High Throughput R&D in Heterogeneous Catalysis, BENTHAM SCIENCE PUBLISHERS, 2014: pp. 288–309. https://doi.org/10.2174/978160805872311401012.
[45] V.B. Thaore, R.D. Armstrong, G.J. Hutchings, D.W. Knight, D. Chadwick, N. Shah, Sustainable production of glucaric acid from corn stover via glucose oxidation: An assessment of homogeneous and heterogeneous catalytic oxidation production routes, Chem. Eng. Res. Des. 153 (2020) 337–349, https://doi.org/10.1016/j.cherd.2019.10.042.
[46] E. Derrien, M. Mounguengui-Diallo, N. Perret, P. Marion, C. Pinel, M. Besson, Aerobic oxidation of glucose to glucaric acid under alkaline-free conditions: au-based bimetallic catalysts and the effect of residues in a hemicellulose hydrolysate, Ind. Eng. Chem. Res 56 (2017) 13175–13189, https://doi.org/10.1021/acs.iecr.7b01571.
[47] S. Solmi, C. Morreale, F. Ospitali, S. Agnoli, F. Cavani, Oxidation of <scp>d</scp> -glucose to glucaric acid using Au/C catalysts, ChemCatChem 9 (2017) 2797–2806, https://doi.org/10.1002/cctc.201700089.
[48] E. Derrien, M. Ahmar, E. Martin-Sisteron, G. Raffin, Y. Queneau, P. Marion, M. Beyerle, C. Pinel, M. Besson, Oxidation of aldoses contained in softwood hemicellulose acid hydrolysates into aldaric acids under alkaline or noncontrolled pH conditions, Ind. Eng. Chem. Res 57 (2018) 4543–4552, https://doi.org/10.1021/acs.iecr.8b00239.
[49] Q. Zhang, Z. Wan, I.K.M. Yu, D.C.W. Tsang, Sustainable production of high-value gluconic acid and glucaric acid through oxidation of biomass-derived glucose: A critical review, J. Clean. Prod. 312 (2021), 127745, https://doi.org/10.1016/j.jclepro.2021.127745.
[50] Q. Zhang, S. Xu, Y. Cao, R. Ruan, J.H. Clark, C. Hu, D.C.W. Tsang, Sustainable production of gluconic acid and glucuronic acid via microwave-assisted glucose oxidation over low-cost Cu-biochar catalysts, Green. Chem. 24 (2022) 6657–6670, https://doi.org/10.1039/D2GC02568J.
[51] J. Teržan, A. Sedminek, Ž. Lavrič, M. Grilc, M. Huš, B. Likozar, Selective oxidation of biomass-derived carbohydrate monomers, Green. Chem. 25 (2023) 2220–2240, https://doi.org/10.1039/D2GC04623G.
[52] G. Gao, S. Feng, Z. Jiang, C. Hu, Q. Zhang, D.C.W. Tsang, Efficient hydrogenation of glucose to polyols over hydrotalcite-derived ptni alloy catalyst under mild conditions, Ind. Eng. Chem. Res 62 (2023) 3140–3150, https://doi.org/10.1021/acs.iecr.2c04313.
[53] J.F. Kornecki, D. Carballares, P.W. Tardioli, R.C. Rodrigues, Á. Berenguer-Murcia, A.R. Alcántara, R. Fernandez-Lafuente, Enzyme production of <scp>d</scp> -gluconic acid and glucose oxidase: successful tales of cascade reactions, Catal. Sci. Technol. 10 (2020) 5740–5771, https://doi.org/10.1039/D0CY00819B.
[54] P. Komáromy, P. Bakonyi, A. Kucska, G. Tóth, L. Gubicza, K. Bélafi-Bakó, N. Nemestóthy, Optimized pH and its control strategy lead to enhanced itaconic acid fermentation by aspergillus terreus on glucose substrate, Fermentation 5 (2019) 31, https://doi.org/10.3390/fermentation5020031.
[55] R.M. Lindeque, J.M. Woodley, The effect of dissolved oxygen on kinetics during continuous biocatalytic oxidations, Org. Process Res Dev. 24 (2020) 2055–2063, https://doi.org/10.1021/acs.oprd.0c00140.
[56] P. Beltrame, M. Comotti, C. della Pina, M. Rossi, Aerobic oxidation of glucose, Appl. Catal. A Gen. 297 (2006) 1–7, https://doi.org/10.1016/j.apcata.2005.08.029.
[57] M. Liu, X. Jin, G. Zhang, Q. Xia, L. Lai, J. Wang, W. Zhang, Y. Sun, J. Ding, H. Yan, C. Yang, Bimetallic AuPt/TiO $_2$ catalysts for direct oxidation of glucose and gluconic acid to tartaric acid in the presence of molecular O $_2$, ACS Catal. 10 (2020) 10932–10945, https://doi.org/10.1021/acscatal.0c02238.
[58] A. Walkowiak, J. Wolska, A. Wojtaszek-Gurdak, I. Sobczak, L. Wolski, M. Ziolek, Modification of gold zeolitic supports for catalytic oxidation of glucose to gluconic acid, Materials 14 (2021) 5250, https://doi.org/10.3390/ma14185250.
[59] G. Kresse, J. Hafner, *Ab initio* molecular dynamics for liquid metals, Phys. Rev. B 47 (1993) 558–561, https://doi.org/10.1103/PhysRevB.47.558.
[60] G. Kresse, J. Hafner, *Ab initio* molecular-dynamics simulation of the liquid-metal–amorphous-semiconductor transition in germanium, Phys. Rev. B 49 (1994) 14251–14269, https://doi.org/10.1103/PhysRevB.49.14251.
[61] G. Kresse, J. Furthmüller, Efficiency of ab-initio total energy calculations for metals and semiconductors using a plane-wave basis set, Comput. Mater. Sci. 6 (1996) 15–50, https://doi.org/10.1016/0927-0256(96)00008-0.
[62] B. Hammer, L.B. Hansen, J.K. Nørskov, Improved adsorption energetics within density-functional theory using revised Perdew-Burke-Ernzerhof functionals, Phys. Rev. B. 59 (1999) 7413–7421, https://doi.org/10.1103/PhysRevB.59.7413.
[63] S. Grimme, J. Antony, S. Ehrlich, H. Krieg, A consistent and accurate ab initio parametrization of density functional dispersion correction (DFT-D) for the 94 elements H-Pu, J. Chem. Phys. 132 (2010), 154104, https://doi.org/10.1063/1.3382344.
[64] P.E. Blöchl, Projector augmented-wave method, Phys. Rev. B 50 (1994) 17953–17979, https://doi.org/10.1103/PhysRevB.50.17953.
[65] G. Kresse, D. Joubert, From ultrasoft pseudopotentials to the projector augmented-wave method, Phys. Rev. B. 59 (1999) 1758–1775, https://doi.org/10.1103/PhysRevB.59.1758.
[66] J. Kästner, P. Sherwood, Superlinearly converging dimer method for transition state search, J. Chem. Phys. 128 (2008), 014106, https://doi.org/10.1063/1.2815812.
[67] P. Xiao, D. Sheppard, J. Rogal, G. Henkelman, Solid-state dimer method for calculating solid-solid phase transitions, J. Chem. Phys. 140 (2014), 174104, https://doi.org/10.1063/1.4873437.
[68] S. Mongkholkeaw, A. Songsasen, T. Duangthongyou, K. Chainok, S. Suramitr, W. Wattanathana, B. Wannalerse, Crystal structure, Hirshfeld surface analysis and computational study of 2-chloro- *N* -[4-(methylsulfanyl)phenyl]acetamide, Acta

Crystallogr E Crystallogr Commun. 76 (2020) 594–598, https://doi.org/10.1107/S2056989020002960.
[69] A. Maeland, T.B. Flanagan, Lattice spacings of gold–palladium alloys, Can. J. Phys. 42 (1964) 2364–2366, https://doi.org/10.1139/p64-213.
[70] B.N. Wanjala, J. Luo, R. Loukrakpam, B. Fang, D. Mott, P.N. Njoki, M. Engelhard, H.R. Naslund, J.K. Wu, L. Wang, O. Malis, C.-J. Zhong, Nanoscale alloying, phase-segregation, and core−shell evolution of gold−platinum nanoparticles and their electrocatalytic effect on oxygen reduction reaction, Chem. Mater. 22 (2010) 4282–4294, https://doi.org/10.1021/cm101109e.
[71] W. Zhan, J. Wang, H. Wang, J. Zhang, X. Liu, P. Zhang, M. Chi, Y. Guo, Y. Guo, G. Lu, S. Sun, S. Dai, H. Zhu, Crystal structural effect of AuCu alloy nanoparticles on catalytic CO oxidation, J. Am. Chem. Soc. 139 (2017) 8846–8854, https://doi.org/10.1021/jacs.7b01784.
[72] G.-X. Kong, X.-J. Ma, Q.-J. Liu, Y. Li, Z.-T. Liu, Structural stability, elastic and thermodynamic properties of Au–Cu alloys from first-principles calculations, Phys. B Condens Matter 533 (2018) 58–62, https://doi.org/10.1016/j.physb.2018.01.003.
[73] S. Ogawa, D. Watanabe, Electron diffraction study on the ordered alloy CuAu, J. Phys. Soc. Jpn. 9 (1954) 475–488, https://doi.org/10.1143/JPSJ.9.475.
[74] A. Borodziński, M. Bonarowska, Relation between Crystallite Size and Dispersion on Supported Metal Catalysts, Langmuir 13 (1997) 5613–5620, https://doi.org/10.1021/la962103u.
[75] Copper, Silver and Gold, in: Chemistry of the Elements, Elsevier, 1997, pp. 1173–1200, https://doi.org/10.1016/B978-0-7506-3365-9.50034-1.
[76] Nickel, Palladium and Platinum, in: Chemistry of the Elements, Elsevier, 1997, pp. 1144–1172, https://doi.org/10.1016/B978-0-7506-3365-9.50033-X.
[77] G. Bergeret, P. Gallezot, Particle size and dispersion measurements, in: Handbook of Heterogeneous Catalysis, Wiley-VCH Verlag GmbH & Co. KGaA, Weinheim, Germany, 2008, https://doi.org/10.1002/9783527610044.hetcat0038.
[78] M.P. Casaletto, A. Longo, A. Martorana, A. Prestianni, A.M. Venezia, XPS study of supported gold catalysts: the role of Au0 and Au+δ species as active sites, Surf. Interface Anal. 38 (2006) 215–218, https://doi.org/10.1002/sia.2180.
[79] S. Brunauer, P.H. Emmett, E. Teller, Adsorption of gases in multimolecular layers, J. Am. Chem. Soc. 60 (1938) 309–319, https://doi.org/10.1021/ja01269a023.
[80] N.K. Gupta, S. Nishimura, A. Takagaki, K. Ebitani, Hydrotalcite-supported gold-nanoparticle-catalyzed highly efficient base-free aqueous oxidation of 5-hydroxymethylfurfural into 2,5-furandicarboxylic acid under atmospheric oxygen pressure, Green. Chem. 13 (2011) 824, https://doi.org/10.1039/c0gc00911c.
[81] K. Frey, D.J. Schmidt, C. Wolverton, W.F. Schneider, Implications of coverage-dependent O adsorption for catalytic NO oxidation on the late transition metals, Catal. Sci. Technol. 4 (2014) 4356–4365, https://doi.org/10.1039/C4CY00763H.
[82] F.W. Schenck, Glucose and Glucose-Containing Syrups, in: Ullmann's Encyclopedia of Industrial Chemistry, Wiley, 2006, https://doi.org/10.1002/14356007.a12_457.pub2.
[83] E. Derrien, M. Mounguengui-Diallo, N. Perret, P. Marion, C. Pinel, M. Besson, Aerobic oxidation of glucose to glucaric acid under alkaline-free conditions: au-based bimetallic catalysts and the effect of residues in a hemicellulose hydrolysate, Ind. Eng. Chem. Res 56 (2017) 13175–13189, https://doi.org/10.1021/acs.iecr.7b01571.
[84] J.M. Gottfried, K.J. Schmidt, S.L.M. Schroeder, K. Christmann, Spontaneous and electron-induced adsorption of oxygen on Au(110)-(1×2, Surf. Sci. 511 (2002) 65–82, https://doi.org/10.1016/S0039-6028(02)01555-8.
[85] S. Rautiainen, P. Lehtinen, J. Chen, M. Vehkamäki, K. Niemelä, M. Leskelä, T. Repo, Selective oxidation of uronic acids into aldaric acids over gold catalyst, RSC Adv. 5 (2015) 19502–19507, https://doi.org/10.1039/C5RA01802A.
[86] M.M. Montemore, M.A. van Spronsen, R.J. Madix, C.M. Friend, O_2 activation by metal surfaces: implications for bonding and reactivity on heterogeneous catalysts, Chem. Rev. 118 (2018) 2816–2862, https://doi.org/10.1021/acs.chemrev.7b00217.
[87] M.P. Hyman, J.W. Medlin, Effects of electronic structure modifications on the adsorption of oxygen reduction reaction intermediates on model Pt(111)-alloy surfaces, J. Phys. Chem. C. 111 (2007) 17052–17060, https://doi.org/10.1021/jp075108g.
[88] J. Lee, B. Saha, D.G. Vlachos, Pt catalysts for efficient aerobic oxidation of glucose to glucaric acid in water, Green. Chem. 18 (2016) 3815–3822, https://doi.org/10.1039/C6GC00460A.